FaAA-84-3-14
PA07396/GKD-03340A(2)

DESIGN REVIEW OF CONNECTING RODS FOR TRANSAMERICA DELAVAL DSRV-4 SERIES DIESEL GENERATORS

****

The report is final, pending confirmatory reviews required by FaAA's QA operating procedures.

****

Prepared by

Failure Analysis Associates
Palo Alto, California

Prepared for

TDI Diesel Generator Owners Group

May 1984

STATEMENT OF APPLICABILITY

This report addresses the structural integrity of connecting rods in the Transamerica Delaval Inc. (TDI) DSRV-16-4, DSRV-20-4, and DSRV-12-4 V-series engines. The articulated connecting rod design analyzed in this report is the same in all TDI R-4 V-series engines. However, the bolting securing the pin joint to the articulated and master connecting rods is different in the DSRV-16-4 engines installed in Mississippi Power & Light Company's Grand Gulf Nuclear Station in that the link rod box is secured to the master rod by 1 $^{7}/_{8}$-inch diameter bolts. Other TDI owners have engines with 1 $^{1}/_{2}$-inch diameter bolts in this joint. Both versions are evaluated in this report.

EXECUTIVE SUMMARY

The Transamerica Delaval Inc. DSRV-4 articulated connecting rod assembly consists of a link rod box containing the pin bearing bolted to the master rod across a lapped serrated joint. The upper pair of bolts nearest the connecting rod bearing has been prone to fatigue failure, and in several instances fatigue cracks have been found in the bolt holes. Two different bolt diameters, 1 $^{7}/_{8}$-inch and 1 $^{1}/_{2}$, and two levels of pretorque for both diameters have been employed in service.

The inertial and gas pressure loading has been calculated for the connecting rod assembly and applied to a two dimensional finite element model of the rod box to master rod assembly. The stress range for the 1 $^{7}/_{8}$-inch bolt holes is greater than that for the 1 $^{1}/_{2}$-inch bolt holes by approximately 8%. At the high levels of pretorque, 2600 and 1700 ft-lb, respectively, fracture mechanics calculations show that the stress intensity range at thread roots of 1 $^{7}/_{8}$-inch bolt holes is in the range of the lower limit of fatigue crack propagation threshold.

The stress calculations assumed perfect contact along the lapped joint under the specified bolt pretorque. Lack of perfect contact could result in fretting wear, relaxation of bolt preload and increased stress range in the bolts and bolt holes.

In view of the criticality of this assembly, it is recommended that inspections of the bolts and bolt holes be carried out at regular intervals. Based on the resolution of eddy current inspection, this interval should not exceed 200 hours of operation at full load, 248 hours at 85% load, or 286 hours at 75% load. The breakaway torque should also be measured, and the fit between the mating surfaces of the serrated joint should be inspected for signs of fretting wear. In the event of fretting indications or low breakaway bolt torques, the bolts and contact areas require more detailed examination. An ultrasonic bolt stress measurement device is preferable to measurement of breakaway torque.

The rod eye and the rod-eye bushing are subject to the same loads and acceptance/rejection criteria as reported for the inline DSRV-4 connecting rod.

TABLE OF CONTENTS

Page

STATEMENT OF APPLICABILITY.....i

EXECUTIVE SUMMARY.....ii

1.0 INTRODUCTION 1-1

1.1 Service Experience.....1-2
1.2 Observations of Cracked Rod.....1-2

Section 1 References.....1-3

2.0 CONNECTING ROD EVALUATION.....2-1

2.1 Rod Bow Analysis.....2-1
2.2 Analysis Of The Lower Connecting Rod Assembly.....2-2
2.2.1 Finite Element Modeling.....2-3
2.2.2 Loading Conditions.....2-6
2.2.3 Finite Element Stress Analysis Results.....2-7
2.2.4 Fracture Mechanics Analysis of Bolt Holes.....2-9
2.3 Rod-Eye Analysis.....2-14

Section 2 References.....2-13

3.0 CONCLUSIONS

APPENDIX A: Derivation of Piston Acceleration for Articulated Rod.....A-1

APPENDIX B: Component Task Descriptions.....B-1

1.0 INTRODUCTION

This report addresses the structural integrity of connecting rods in the Transamerica Delaval Inc. (TDI) DSRV-4 16, 20, and 12 cylinder engines used in emergency generator sets in nuclear power stations.

The connecting rods used in the V-series engines are of an articulated design that operates two pistons off each crank throw. The V-series engine connecting rods have been manufactured with either 1 $^{7}/_{8}$ or 1 $^{1}/_{2}$-inch diameter bolts connecting the link rod box to the master rod. The 1 $^{7}/_{8}$-inch version is installed in the DSRV-16-4 engines at Grand Gulf Nuclear Station; other owners have engines with 1 $^{1}/_{2}$-inch bolts. The master rods have either round or H-shaped shank cross sections.

The function of the connecting rod is to transmit cylinder firing forces from the piston pins to the crankshaft such that the reciprocating forced motion of both pistons is translated into rotation and torque at the crankshaft. The connecting rod must have sufficient column strength and fatigue resistance to withstand repeated cylinder firings and inertial loadings. Both master and link rods must carry cooling and lubricating oil to pistons and piston pin bearings. Finally, the design of the link-rod-box-to-master-rod joint incorporates mating serrations which must be protected from fretting and local stress concentration effects. The configuration of the V-series engine connecting rod is shown in Figure 1-1.

The bushings of the reciprocating bearings in the connecting rod eyes and the crankpin bearing shells have been evaluated in previous reports [1-1, 1-2]. The key subjects of this report are the rod eye, link pin housing, and connecting rod bearing housings.

The Component Task Description for the V-series engine connecting rod is contained in Appendix B. The evaluation focuses on those areas for which service experience indicates a significant incidence of failure. This experience is summarized in Section 1.1.

1.1 Service Experience

The survey of industry experience with DSRV-4 connecting rods summarized in this section has not been independently confirmed by FaAA and, therefore, is not subject to FaAA's usual quality assurance procedures.

TDI has supplied information concerning two failure mechanisms that have been experienced in non-nuclear installations.

The first mechanism is fatigue failure of the link rod bolts resulting from loss of bolt preload. The problem and its solution were addressed by TDI in Service Information Memo No. 349, dated September 18, 1980 [1-3]. According to this SIM, engines manufactured between 1972 and February, 1980, may have been shipped with an insufficient locating dowel counterbore depth in the link rod or link pin, resulting in clearance between the link rod and link pin as assembled. Under firing load, this locating dowel will yield, allowing the above clearance to disappear and resulting in loose link rod bolts. There must be zero clearance under the specified bolt torque of 1050 ft-lb, in spite of SIM 349, which recommends checking clearance with a 0.0015-inch feeler gage.

The second mechanism is fatigue cracking of the connecting rod bolts and/or the link rod box in the mating threads. Figure 1-2 shows schematically the location and origin of the crack path. TDI indicated knowledge of numerous instances of bolt or rod fatigue of this nature where low assembly torque values were specified. FaAA examined one crack in a rod which was assembled with a modified specification of a higher bolt torque, documented in the following section. TDI attributed these rod cracks to "thread fretting". This "thread fretting" was concluded by TDI to result from distortion of the rod and bolt under operating loads in the area of the mating threads which could occur if the bolts had been installed with the originally specified lower preloads. TDI produced results of a static load strain gage test of an assembled connecting rod with 1 $^{7}/_{8}$-inch diameter bolts that indicated the alternating stresses were reduced 25% by increasing the assembly torque from 2200 ft-lb to 3200 ft-lb. According to TDI, the effect of this increased preload is to stiffen the threaded joint by distributing load over more

threads, thus reducing the concentrated stress both in the bolt and the bolt hole. The current torque specification for the 1 $^{7}/_{8}$-inch diameter bolts is 2600 ft-lb [1-4].

Later DSRV-16-4 engines have connecting rods with 1 $^{1}/_{2}$-inch diameter bolts. At the present time only the four DSRV-16-4 engines at Grand Gulf Nuclear Station are reported to have the 1 $^{7}/_{8}$-inch diameter design in emergency generator sets in nuclear installations. TDI indicated that the design change to the smaller diameter bolts was intended to provide greater section thickness in the link rod box around the bolt threads [1-5]. The specified torque for the 1 $^{1}/_{2}$-inch diameter bolts is 1700 ft-lb. [1-4].

According to TDI [1-5], there have been no reports of cracked connecting rods with either bolt size when the specified torque is applied during assembly. FaAA has been unable to confirm this conclusion to date, since two cracked rods have been found in a marine engine assembled and operated during the time period when the higher specified torque level was apparently in effect. However, recent inspection of all 8 connecting rods for bolt and bolt hole cracking in the 1A engine at Catawba Nuclear Power Station after more than 800 hours of operation disclosed no relevant indications.

Another potential problem reportedly encountered with H-section connecting rod shanks is distortion leading to axial misalignment. This condition is analyzed in Section 2.1.

1.2 Articulated Connecting Rod Failure

A metallurgical failure analysis was performed on a failure which occurred in the link rod box at the lower pair of four bolt holes. This particular articulated connecting rod was removed from a TDI DMRV-12-4 engine. The location of the failure is shown in Figure 1-2.

Metallurgical and mechanical tests were performed on material removed from the link rod box. This material, AISI 4140 or AISI 4142, had a yield strength of ~88.5 ksi, ultimate strength of ~115 ksi, and elongation of ~20%. The average measured hardness was 20 HRC (230 BHN). The metallurgical

microstructure was that of a well-tempered martensitic structure, which is to be anticipated with the measured hardness and strength values.

The failure was the result of progressive fatigue crack growth from a threaded bolt hole. A photograph showing the entire fracture surface is shown in Figure 1-3. Fractography, geometry, and coloration indicate the primary origin was at the root of a thread. The origin, Site A, is shown in the macrophotograph, Figure 1-4.

A secondary origin, Site B, occurs at a step in the thread flank. This step was probably introduced when the bolt was torqued, or in the event bolt fracture preceded the cracking in the rod, when the bolt fractured. No record of the condition of the bolt from this hole upon disassembly was available. The sharp step acted as a stress concentrator which subsequently acted as the crack initiator. Both cracks initiated at stress concentrators that showed evidence of yielding. No evidence of fretting was observed on the thread surfaces. Greater than 75% of the fracture is attributable to fatigue crack growth.

Section 1 References

1-1 Failure Analysis Associates, "Design Review of Connecting Rods of Transamerica Delaval Inline DSR-48 Emergency Diesel Generators," FaAA-84-3-13, April 1984.

1-2 Failure Analysis Associates, "Design Review of Connecting Rod Bearing Shells for Transamerica Delaval Enterprise Engines," FaAA-84-3-1, March 12, 1984.

1-3 Service Information Memo No. 349, Transamerica Delaval Inc., Sept. 18, 1980.

1-4 TDI Owners Manual, Cleveland Electric Company.

1-5 Maurice Lowrey, Transamerica Delaval Inc., personal communication, May 1984.

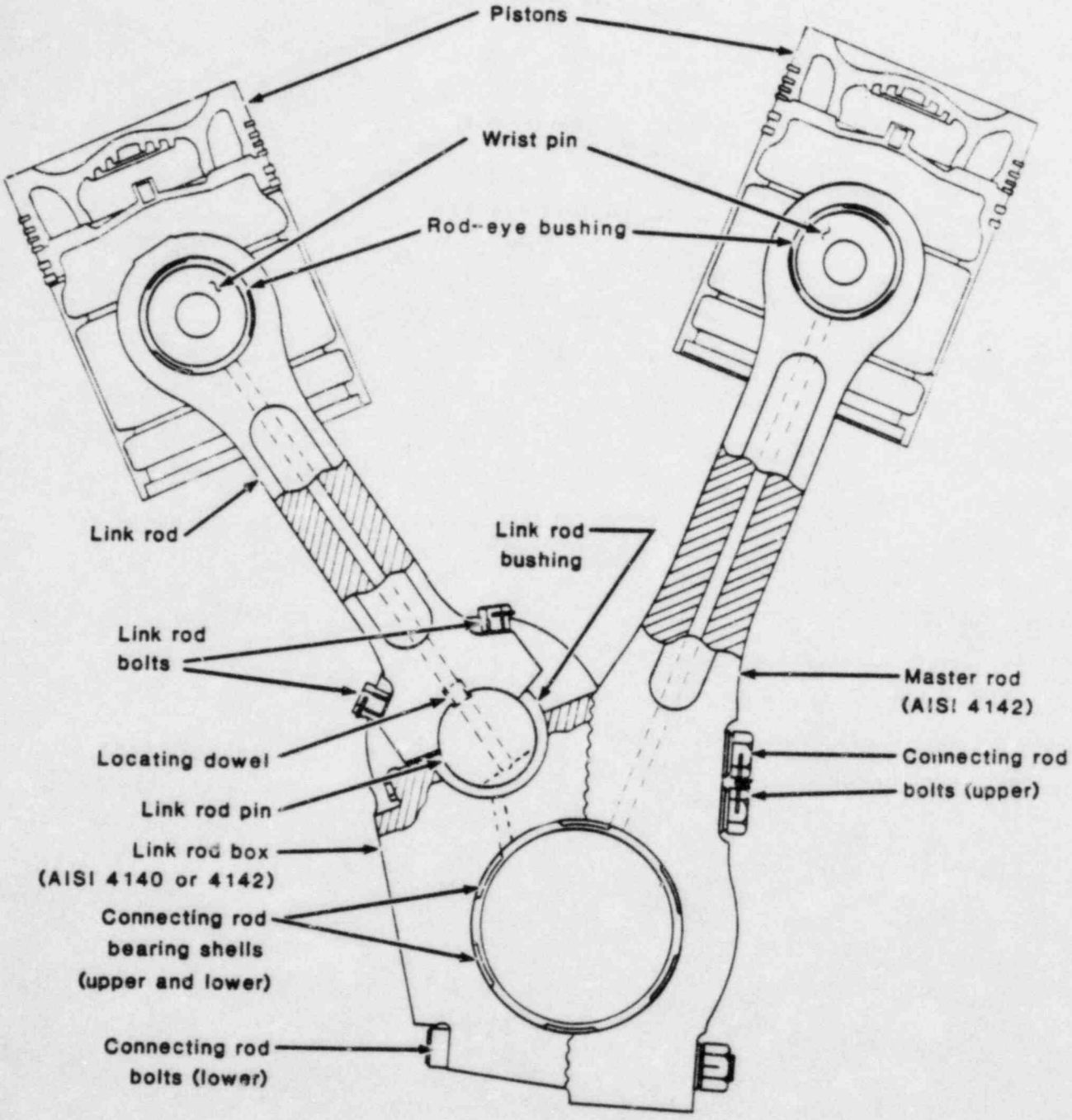

Figure 1-1. V-engine connecting rod, model RV-4 engine.

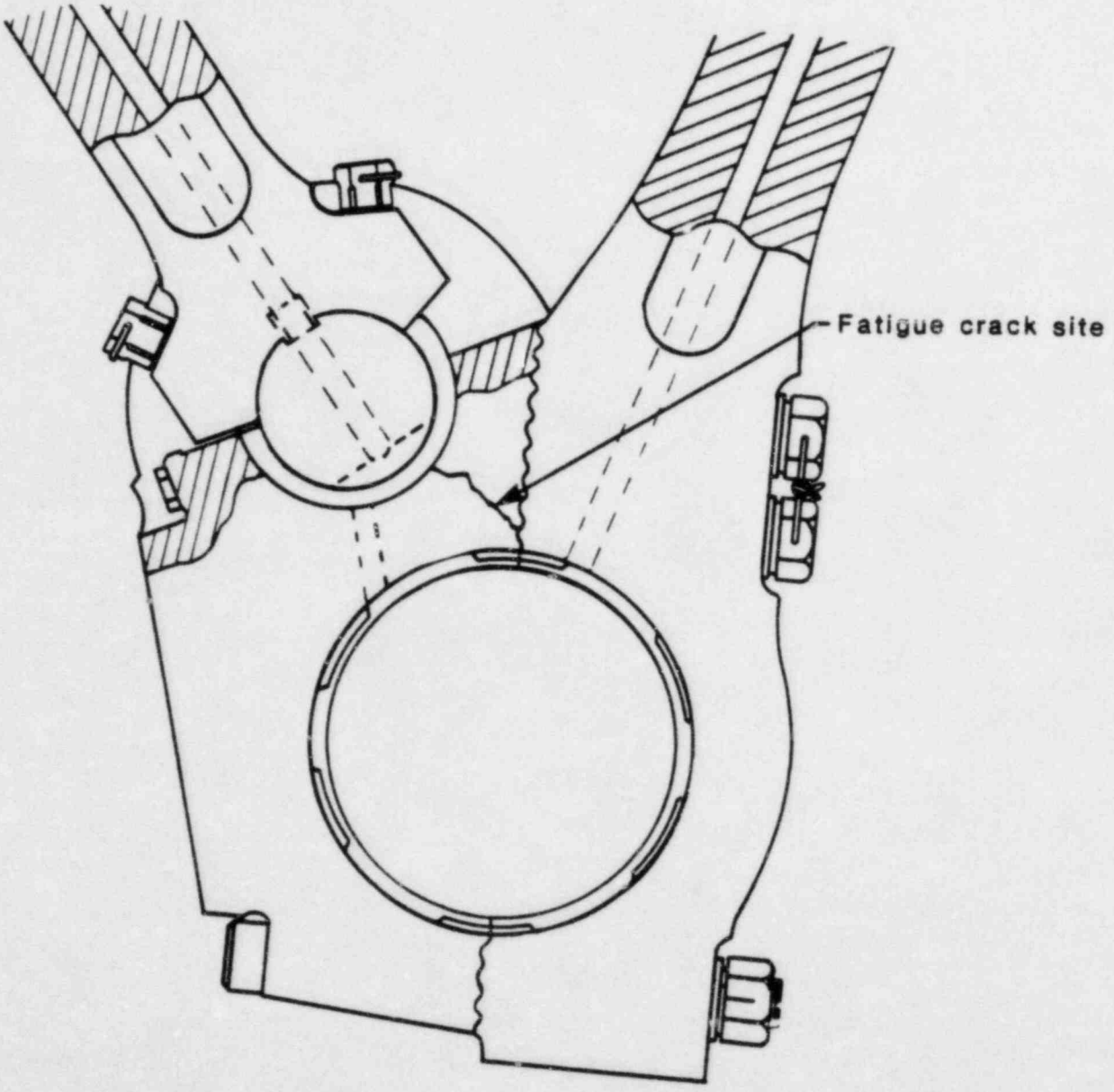

Figure 1-2. Schematic showing fatigue crack origin and path.

Figure 1-3. Surface photograph of the articulated link rod box fracture surface. 7396-LT1-39-84-7541-001-FS

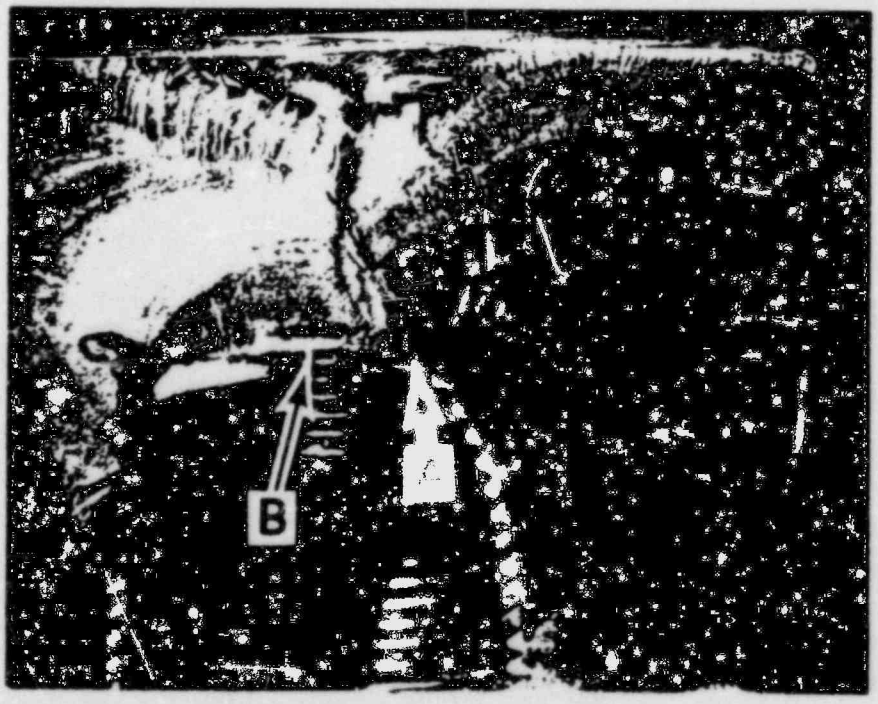

Figure 1-4. Macrophotograph showing the location of the primary fatigue origin (A) and secondary fatique origin (B) on the articulated link rod box. 7396-LT3-39-84-7541-001-FS

2.0 CONNECTING ROD EVALUATION

An analysis was performed (Section 2.1) to determine the degree of centerline bow that can be tolerated by the V-Series engine (RV-4) H-section connecting rod. In Section 2.2, the finite element stress and fracture mechanics analyses of the lower connecting rod assembly are presented. The fatigue resistance of the rod eye is discussed in Section 2.3

2.1 Rod Bow Analysis

The connecting rods in the TDI RV-4 Series engines may incorporate either a round machined shank, or an as-forged, H-section shank (see Figure 2-1). Forging practices may have resulted in the manufacture of rods with slightly curved centerlines. The purpose of this analysis is to determine what degree of centerline bow can be tolerated without exceeding the requirements of related components. Specifically, the axial misalignment of the connecting rod bearing resulting from flexure of a bent or bowed connecting rod with various degrees of centerline bow is calculated and related to published standards [2-1] to determine the acceptance/rejection criterion for this condition.

The forging practice mentioned above may be that of placing a hot forging on its side (bearing axis vertical) supported only on either end to cool after forming. At forging temperatures the material could sag under its own weight, and the resultant bend could be in the direction which would lead to the greatest bearing misalignment.

If misalignment is slight compared to bearing clearance, as it is in this case, axial misalignment is analogous to crankpin taper wherein the amount of taper is equivalent to twice the amount of misalignment. It has been suggested that crankpin taper be limited to 0.0003 inch over the length of a bearing more than 2 inches in diameter to afford optimum bearing life [2-1]. Therefore, this analysis considers an axial misalignment of 0.00015 inch to be the maximum allowable.

Axial misalignment causes the oil film pressure profile of a journal bearing to shift such that a restoring force is generated [2-2]. The entire oil film pressure profile is skewed, with pressures being higher on the side of the bearing where the oil film thickness is reduced by the tipping of the bearing housing relative to the shaft. A relationship exists between the size of the bearing, its clearance and loading, the degree of misalignment, and the equivalent offset of the reaction forces. In the TDI model RV-4 engine at full load, an axial misalignment of a connecting rod bearing of 0.00015 inch over the length of the bearing will produce an offset in the position of reaction forces of 0.029 inch [2-2]. This offset, then, defines the equilibrium position of a connecting rod at maximum axial misalignment.

For the example of a bowed connecting rod, the offset can further be broken down into two components. The components are, first, that offset which results directly from misalignment or tilting of the connecting rod and, secondly, the further offset that develops as the result of loading a curved beam in compression. The tilting is a simple geometric relationship and accounts for 0.010 inch of the allowable 0.029 inch of offset. Therefore, the balance of 0.019 inch of offset is the maximum allowable transverse motion of the connecting rod-eye with respect to the bearing bore that can be tolerated by the system. Solving for the degree of bow that yields this offset using curved beam equations [2-3] reveals that the TDI model RV-4 engine can tolerate a centerline bow in an H-section connecting rod of up to 0.47 inch.

2.2 Analysis of the Lower Connecting Rod Assembly

A finite element (FE) stress analysis of the lower connecting rod assembly is discussed in this section. This analysis was performed to assess the range of cyclic stresses caused by the cylinder gas pressure plus dynamic loads exerted on the connecting rod. Emphasis was on the region of the four upper bolts (Figure 2-2). A fracture mechanics analysis was subsequently performed based on the FE stress analysis results to assess whether or not the cyclic stresses in connecting rods can cause a fatigue failure.

2.2.1 Finite Element Modeling

A two dimensional FE stress analysis of a V-engine connecting rod was performed. The model was developed with the interactive mesh generation code, Patran [2-4] and the analysis performed using the MARC [2-5] general purpose finite element code. A plane-stress analysis was performed selecting eight-node isoparametric elements [2-6]. These elements provide quadratic displacement fields (linear strain variation within the element) and model the curved edges of the crankpin hole and link pin hole. Figure 2-2 shows the lower connecting rod assembly model and Figure 2-3 shows the finite element mesh. The mesh consists of 289 elements and 948 nodes. The model includes the lower portion of the master rod and the link rod box assembly. The interface between the master rod and the link rod box, indicated by the serrated line in Figure 2-2, is modeled with gap elements. These elements allow separation of the two sides. However, because of the serrated attachment, it was decided to assume no relative shear displacement could occur. Actually, relative displacement across the serrated joint is able to occur between the tangents to the tooth profile at the pitch line, an angle of 45°. The master rod and link rod box are connected with bolts above and below the crankpin as illustrated in Figure 2-2. Bolts below the crankpin extend entirely through the connecting rod assembly. Therefore, any prestressing of these bolts will create compressive stresses in the connecting rod itself; on the other hand, tightening of the bolts located above the crankpin would cause tensile stresses near the threads in the link rod box.

The bolts were represented by truss elements, as in Figure 2-4, and bolt prestresses were modeled by applying a thermal strain to the bolt. To account for the reduced stiffness due to the bolt holes, the regions of the 2-D mesh which included the bolts were represented by equivalent material with Young's modulus, E_{eq}, given by the following equation:

$$E_{eq} = E\left(1 - \frac{n\pi D}{4h}\right)$$

where

E = the Young's modulus of the connecting rod = 29 x 10^6 psi

D = the diameter of the bolt hole = 1.906 inch (for 1 $^7/_8$-inch bolt)

h = the thickness of the connecting rod = 6.941 inch

n = the number of bolts through the thickness = 2

This representation is common in situations where it is necessary to approximate a three-dimensional geometry by a two-dimensional model. The model developed here thus represents the load in the shank of the bolt from the underside of the head to the middle thread by an elastic tension member of the same axial stiffness as the bolt. Within the width of the elements representing the bolt holes, the longitudinal and transverse stiffnesses of the rod were adequately represented by the reduced equivalent modulus, and no stiffening effect of the bolt was assumed, as is reasonable in view of the radial clearance between the bolt and the bolt hole. In the region of the mating threads, the bore of the hole is to some extent more resistant to distortion because of the ability to transmit stresses across the pitch diameter. According to TDI [1-5] this is the primary effect of the increased bolt preload. It is apparently intended that the threads closest to the head of the bolt deform plastically and transmit more contact force to adjacent threads. This effect was bounded in our analysis by first assuming that the mating threads exerted no reinforcing effect and then by representing the region of the mating threads as solid metal, i.e., no hole. The effect of these bounding assumptions on the cyclic stress range in the hole surface along the axis of the hole is less than 5%.

In addition to the stresses caused by tightening of the bolts, large cyclic loads are exerted on the connecting rod assembly due to the gas pressure in the cylinders and the inertial loads due to the mass of the pistons and the connecting rods.

Inertial loads were determined by lumping masses at the two pistons and the crankpin and determining the acceleration of these points from the kinematics of the V-engine. The mass lumped at the center of the crankpin has a circular motion, causing a centrifugal force equal to:

$$F_{I_C} = m_c \omega^2 R,$$

where

F_{I_C} = the centrifugal force = 56301 lbs

m_c = mass lumped at the crankpin = 933 lbs (weight)

ω = the angular velocity 2π (450) radians/minute

R = the radius of the rotation, i.e., the distance between the centers of the crankpin and the crankshaft = 10.5 inch

The direction of the centrifugal force is radially outward from the center of the crankshaft to the center of the crankpin. This force was modeled in the finite element analysis by distributed body forces. Appendix A describes the derivation of the acceleration of the pistons for a V-engine with an articulated rod configuration as in the TDI RV-4 diesel engines. A computer program called CONROD was written to implement this analysis and determine the inertial forces as a function of crank angle. CONROD combines the gas pressure and inertial loads on the piston. On the master rod the combined gas pressure and inertial loads are applied at the surface designated by C in Figure 2-2. The force along this face is predominantly axial with a small shear component and a moment. The force acting on the link rod due to the gas pressure and inertia is primarily axial since rotary inertia of the link rod is negligible; this load is transferred to the connecting rod assembly at the link pin with an oil film pressure distribution, assumed to be a cosine pressure distribution.

The applied forces are balanced by an oil film pressure distribution on the crankpin also approximated by a cosine distribution. Although the reaction force at the crankpin is in equilibrium with the applied forces, boundary constraints are needed for the finite element analysis. Therefore, Points A and B, as shown in Figure 2-2 below the crankpin, were constrained in the vertical direction, and Point A was additionally constrained in the horizontal direction. As expected, the reactions at Points A and B were very small.

Geometry. The dimensions of the FE model are based on those given on numerous TDI drawings. Figure 2-5 shows these dimensions. The bolts connecting the master rod and link rod box are of either 1 $^7/_8$-inch diameter or 1 $^1/_2$-inch diameter.

Material Properties. The master rod and the link rod box are made from 4142 Steel [2-7] which has the following properties:

Young's Modulus $E = 29{,}000$ ksi
Poisson's Ratio $\nu = 0.3$
Yield Stress $\sigma_y = 88.61$ ksi
Ultimate Stress $\sigma_u = 114.94$ ksi

Materials A and C shown in Figure 2-2 were assigned the above properties. The region of the bolt hole (material B) was modeled with a reduced equivalent Young's Modulus:

For the 1 $^7/_8$-inch diameter bolt:

$$E_{eq} = 29{,}000\left(1 - \frac{\pi(1.906)}{4(3.4705)}\right) = 16{,}491 \text{ ksi},$$

and for the 1 $^1/_2$-inch diameter bolt:

$$E_{eq} = 29{,}000\left(1 - \frac{\pi\,(1.5)}{4\,(3.4705)}\right) = 19{,}156 \text{ ksi}$$

The Poisson's ratio was assumed to be unchanged.

2.2.2 Loading Conditions

Combined gas pressure and inertial loads, plus bolt prestresses, are exerted on the lower connecting rod assembly. The load conditions analyzed are described next.

Bolt Prestress. The master rod and the link rod box are connected with either 1 $^7/_8$-inch diameter or 1 $^1/_2$-inch diameter bolts. The 1 $^7/_8$-inch bolts are torqued to 2600 ft-lbs with a corresponding clamping force of 90 kips [2-8]. The 1 $^1/_2$-inch bolts are torqued to 1700 ft-lbs with a corresponding clamping force of 90 kips. [2-8] This clamping force was based upon data generated by Crane Co. for threaded fasteners lubricated by graphite and oil. The conventionally calculated preload, e.g., according to Shigley, [2-8]

would yield 83 kips and 68 kips respectively. The clamping force is modeled by applying a thermal strain ($\alpha\Delta T$) to the elements representing the bolts. The magnitude* of $\alpha\Delta T$ is chosen such that the resulting force in each bolt is 89.754 kips in the 1 $^{7}/_{8}$-inch diameter bolts and 89.781 kips in the 1 $^{1}/_{2}$-inch bolts.

Gas Pressure Force. The gas pressure in the cylinder at full load was measured at 1° intervals of crank angle from 0° to 720° for the Shoreham diesel engine DG103. This pressure is shown in Figure 2-6. The peak gas pressure in V-engine cylinders was measured at Catawba and Grand Gulf plants to be approximately the same as that of Shoreham's DG103 tested engine.

The force acting on the connecting rod due to the gas pressure is equal to the pressure times the piston area of 227 inch^2.

Inertial Force. Dynamic loads are generated due to the motion of the mass of the pistons and the connecting rod itself. The derivation of these inertial forces is presented in Appendix A.

Load Conditions Analyzed. Several load cases corresponding to specific crank angles are analyzed here to determine the maximum range of cyclic stress that the connecting rod is subjected to at full load. At any crank-angle position the connecting rod will be loaded by a combination of inertial force, gas pressure force, and the bearing reaction. The computer program CONROD computes these forces and their directions. Figure 2-7 shows the forces acting on the connecting rod. The magnitude and orientation of these forces change as a function of the crank angle.

Table 2.1 lists the load cases anaylzed, along with the different loads considered for the analysis. The crank angles shown in Table 2.1 are measured from the TDC of the articulated rod during its combustion stroke.

---

* $\alpha\Delta T$ is a negative value.

2.2.3 Finite Element Stress Analysis Results

Tables 2.2 and 2.3 summarize results of the finite element stress analysis. From the results of the finite element analysis, it was found that:

- Maximum tensile stresses in the area investigated are produced in the link rod box near TDC of the link rod when peak firing pressure occurs.

- Maximum stresses occur at the crankpin hole near a line connecting the crankpin center to the link pin center.

- Tensile stresses in the connecting rod result from the noncolinear loads exerted at the link pin hole and the reaction on the crankpin hole. This offset in loads produces a bending moment which causes tensile stresses in the link rod box above the crankpin and adjacent to Bolt 1 (Figure 2-2).

- Nominal stresses near the upper bolts are slightly lower than at the crankpin hole; however, because of the presence of the threads, higher stresses occur near the bolts due to stress concentration effect of the threads.

- Maximum compressive stresses in the element adjacent to Bolt 1 occur for Load Case 17 which corresponds to the 185° crank angle after TDC of the link rod.

- The angle of the bearing pressure distribution along the crankpin hole has a relatively minor influence on the maximum stresses produced near Bolt 1. By reducing the angle of pressure distribution from 120° to 60° (i.e., concentrating the reaction force at the crankpin hole), the maximum stress is effectively unchanged.

- Timing of the peak gas pressure has a small effect on stresses in the link rod box. Maximum principal stress at Bolt Hole No. 1 increases from 16.38 ksi to 17.55 ksi when peak pressure occurs 2° after TDC instead of 7° after TDC. For peak pressure occurring 12° after TDC, stresses are reduced to 15.46 ksi at Bolt Hole No. 1.
- For the 1 $^{7}/_{8}$-inch diameter bolt design, the maximum range (i.e., double amplitude) of cyclic principal stress at the bolt hole is 9.88 ksi. The direction of this stress is 49.4° to the axis of the bolt hole (see Figure 2-2).

- For the 1 $^{1}/_{2}$-inch diameter bolt, the maximum range of cyclic stress at the bolt hole is 9.01 ksi. The direction of this stress is 57.8° to the global axis of the bolt hole. This angle agrees well with the direction normal to the fracture surface examined (56°).

- The maximum cyclic stress range occurs at the link pin bearing hole at the minimum ligament between the crankpin hole and link pin hole. The maximum stress range here is 28.36 ksi. There are no stress concentration effects assumed at this location because the oil hole is removed sufficiently to produce a negligible effect. Therefore, this stress range is less critical than that at the bolt hole.

Figure 2-8 shows the distribution of the stress range for both 1 $^{7}/_{8}$-inch bolt and 1 $^{1}/_{2}$-inch bolt configurations in the bolt hole region of Bolt 1. Elements in the bolt hole region are shown in Figure 2-9.

2.2.4 Fracture Mechanics Analysis of Bolt Holes

In this section, crack initiation at the bolt holes and fatigue crack propagation rates are assessed. The cyclic stress intensity factor, which controls crack growth rate, is based on the maximum cyclic stress range determined from the FE analysis. The cyclic stress intensity factor is compared

$$F_{I1} = 0.60$$

$$\Delta K_I = 9.88 \sqrt{\pi\ (.043)}\ 0.60 = 2.179\ \text{ksi}\sqrt{\text{in}}$$

The effective stress intensity is given by [2-10]:

$$\Delta K_{eff} = \left(\frac{1.5}{1.5 - R}\right) \Delta K_I$$

where

$$R = \text{the ratio of the minimum to maximum stress} = \frac{\sigma_{min}}{\sigma_{max}}$$

For stresses exceeding the flow stress, the R ratio is defined as:

$$R = \frac{\sigma_{flow} - \Delta\sigma}{\sigma_{flow}} = \frac{101.8 - 9.88}{101.8} = 0.9$$

The flow stress is defined as:

$$\sigma_{flow} = \frac{\sigma_{ultimate} + \sigma_{yield}}{2} = \frac{114.94 + 88.6}{2} = 101.8\ \text{ksi}$$

Hence, for the 1 $^{7}/_{8}$-inch diameter bolt, the stress intensity factor range is:

$$\Delta K_{eff} = \frac{1.5}{(1.5 - 0.9)}\ 2.179$$

$$= 5.474\ \text{ksi}\ \sqrt{\text{in.}}$$

This effective stress intensity factor range is very close to the threshold of fatigue which ranges from 5.0 to 7.5 ksi $\sqrt{\text{in.}}$

Fatigue Crack Propagation (1 $^{1}/_{2}$-inch Diameter Bolt)

The maximum range of principal stress computed by the FE analysis at the bolt hole is:

$$\Delta\sigma_{max} = 9.01\ \text{ksi}$$

with the fatigue threshold for the connecting rod material (4142 Steel) [2-7] to assess whether or not fatigue crack propagation is possible.

Fatigue Initiation

The bolt prestress creates a large mean stress. Locally, yield or above yield stresses occur near the first few threads. Because of this yield level mean stress near the Bolt Hole No. 1 threads, fatigue crack initiation is possible in this location. The next section addresses whether fatigue crack propagation is possible by comparing the effective stress intensity factor range to the fatigue threshold.

Fatigue Crack Propagation (1 $^{7}/_{8}$-inch Diameter Bolt)

The maximum range of principal stress computed by the FE analysis at the bolt hole is:

$$\Delta\sigma_{max} = 9.88 \text{ ksi}$$

To compute the cyclic stress intensity factor, ΔK_I, assume a crack model which has a series of edge cracks, each with length a and separated by a distance of 2h [2-9]. The cyclic stress intensity factor is given by:

$$\Delta K_I = \Delta\sigma_{max}\sqrt{\pi a} \quad F_{I1}(s)$$

where

$F_{I1}(s)$ is a parameter which characterizes the assumed crack configuration model [2-9].

$$s = \frac{a}{a + h}$$

For a 1 $^{7}/_{8}$-inch diameter bolt:

a = thread depth = 0.043 inch

2h = thread pitch = 0.0833 inch

$$s = \frac{.043}{.043 + .0833} = 0.508$$

The stress intensity factor is computed assuming a crack model which has a series of edge cracks, each with length a and separated by a distance of 2h [2-9].

The 1 $^1/_2$-inch diameter bolt has the same pitch and thread depth as the 1 $^7/_8$-inch bolt. Hence, for the 1 $^1/_2$-inch bolt the stress intensity factor range is given by:

$$\Delta K_I = 9.01 \quad \sqrt{\pi\ (0.043)}\ \ 0.60 = 1.99 \text{ ksi } \sqrt{\text{in}}$$

The R-ratio equals:

$$R = \frac{101.8 - 9.01}{101.8} = 0.91$$

The effective stress intensity factor for the 1 $^1/_2$-inch bolt is given by:

$$\Delta K_{eff} = \frac{1.5}{1.5 - 0.91}\ 1.99 = 2.549\ (1.99) = 5.072 \text{ ksi } \sqrt{\text{in}}$$

The 1 $^1/_2$-inch bolt is less critical than the 1 $^7/_8$-inch bolt, which has about an 8% higher stress intensity factor range.

The cyclic stress intensity range determined is unaffected by the level of bolt prestress as long as the prestress is sufficient to prevent separation along the master rod and link rod box joint.

The calculations assume perfect contact along the serrated joint under the specified bolt torque. If perfect contact is not achieved, the stress intensity range will be greater than the values calculated above and may exceed the threshold for crack propagation. It is not possible to evaluate the acceptable amount of contact area on the faces of the joint by simplified FE analysis. Therefore, the adequacy of the assembly and consequent susceptibility to fretting and fatigue cracking must be determined by inspection of the bolt holes.

Section 2 References

2-1. Swanger, Lee, "Selection of Crankshaft Materials for Optimum Performance," SME technical paper No. CM80-329.

2-2. Cameron, Alastair, Basic Lubrication Theory. Third Edition.

2-3. Roark, R. J. and Young, W. C., Formulas for Stress and Strain. Fifth Edition McGraw Hill, 1975.

2-4. PDA/Patran-G Computer Program, 1980.

2-5. MARC General Purpose Finite Element Program, Version K, 1983.

2-6. Zienkiewics, O. C., The Finite Element Method. Third Edition, McGraw Hill, 1977.

2-7. Telephone Conversation with Maurice Lowery, Transamerica Delaval, March 9, 1984.

2-8. Torque Manual, Dresser Industries, Inc., Hand Tool Division, Bolt Chart, p. 36.

2-9. Tada, H., Paris, P., and Irwin, G. "The Stress Analysis of Cracks Handbook," Del Research Corporation, June 1973.

2-10. Hopkins, S.W., Rau, C.A., Leverant, G.R., and Yuen, A., "Effect of Various Programmed Overloads on the Threshold for High Frequency Fatigue Crack Growth," ASTM, STP 595, 1976, pp. 125-141.

2-11. "BIGIF Fracture Mechanics Code for Structures" by Failure Analysis Associates, July 1978. EPRI NP-838, pp. 4-26.

2-12. Rolfe S. T., and Barsom, J. M., Fracture and Fatigue Control in Structures Applications of Fracture Mechanics. Prentice Hall Inc., 1977.

2-13. Failure Analysis Associates Report No. FaAA-84-3-13, "Design Review of Connecting Rods of Transamerica Delaval Inline DSR-48 Emergency Diesel Generators," April 1984.

2.3 Rod Eye Analysis

While the overall dimensions of the DSRV-4 connecting rod-eye are the same as those of the inline DSR-48 rod-eye, the cross section of the wall is either larger than or similar to the inline engine rod-eye. The rods in service can either be round or H-section. The round section rod-eyes are the same thickness as the inline engine rod-eyes, whereas the H-section rod has a thicker rod-eye.

The rod-eye bushing is subject to essentially the same loads in both the inline and V-engines. Accordingly, the same inspection procedures and acceptance/rejection criteria previously reported [2-13] apply to the V-engine.

Fatigue Life Prediction

The maximum stress intensity factor determined for the 1 $^{7}/_{8}$-inch and 1 $^{1}/_{2}$-inch diameter bolt connecting rods (5.47 ksi $\sqrt{in}$ and 5.07 ksi $\sqrt{in}$ respectively) lies near the lower side of the available data for the fatigue crack propagation threshold. Therefore, inspection of the Bolt Hole No. 1 thread area is recommended to detect fatigue cracks. However, any inspection procedure at this location is limited to detecting cracks that exceed $^{1}/_{8}$-inch depth. Therefore, it is necessary to determine the remaining life of a connecting rod which has an initial crack at the bolt hole thread of $^{1}/_{8}$-inch depth. The smallest ligament between Bolt Hole No. 1 and the crankpin bearing bore is 0.8 inches. Assuming a maximum tolerable crack depth of $^{1}/_{2}$-inch, the number of hours required for a semielliptic crack [2-11] $^{1}/_{8}$-inch deep to propagate to a $^{1}/_{2}$-inch deep crack is determined.

Numerical crack propagation analysis was performed using the BIGIF code [2-11]. A three-dimensional elliptical surface crack model in a finite body was assumed [2-11, p. 4-26]. Crack propagation rate is based on Paris's rule [2-12] and for this material equals:

$$\frac{da}{dN} = 4.0 \times 10^{-10} \left(\Delta K_I\right)^3$$

where

a = crack length in inches
N = number of cycles
ΔK_I = maximum stress intensity factor range

The above equation applies when the R-ratio ($R = \sigma_{max}/\sigma_{min}$) is zero. The BIGIF program incorporates the effect of nonzero R-ratio.

The numerical analysis shows that a semicircular crack $^{1}/_{8}$-inch deep could grow to a depth of $^{1}/_{2}$-inch in approximately 200 hours of engine operation at full load firing pressure (1579 psig). At lower loads and pressures, the engine operating hours are given in Table 2-4.

TABLE 2.1a

LOADING CONDITIONS ANALYZED

Load Case Number	Crank Angle (Degrees)	Parameters Considered in the Finite Element Analysis			
		Gas Pressure (psig)		Amount of Clamping Force (Percent)*	Angle for Bearing Pressure Distribution (Degrees)
		Link Rod Cylinder	Master Rod Cylinder		
0	-	0	0	100	-
1	0	1485	34	100	120
2	0	1485	34	50	120
3	0	1485	34	10	120
4	715	1317	31	100	120
5	710	1113	31	100	120
6	700	784	36	100	120
7	0	1485	34	100	60
8	715	1485	31	100	60
9	3	1577	36	100	60
10	315	39	1485	100	60
11	0	1485	34	100	60
12	8	1577	36	100	60
13	5	1485	34	100	60
14	315	39	1485	50	60
15	315	39	1485	10	60
16	158	129	49	100	60
17	185	99	56	100	60
18	200	80	54	100	60

* 100% clamping force is:

- 89.754 kips which corresponds to 2600 ft-lb torque on the 1 $^{7}/_{8}$-inch bolts.
- 89.781 kips which corresponds to 1700 ft-lb torque on the 1 $^{1}/_{2}$-inch bolts.

TABLE 2.1b

LOAD CASES ANALYZED

Load Case Number	Crank Angle at (Deg)	Inertial Force at Crank Pin		Bearing Pressure Link Rod Box		Forces and Moments at Master Rod End			Bearing Pressure Reaction at Crank Pin	
		F_{I_C} (kips)	β (Deg)	F_{2y} (kips)	Ψ (Deg)	F_{1y} (kips)	F_{1x} (kips)	F_{1x}*d (kip-in)	R (kips)	θ (Deg)
0	-	-	-	-	-	-	-	-	- -	
1	0	56.3	4.1	279.05	5.81	-25.586	-8.222	-191.43	202.338	10.95
2	0	56.3	4.1	279.05	5.81	-25.586	-8.222	-191.43	202.338	10.95
3	0	56.3	4.1	279.05	5.81	-25.586	-8.222	-191.43	202.338	10.95
4	715	56.3	-1.69	241.66	6.2	-31.16	-7.6	-176.83	164.78	16.443
5	710	56.3	-7.56	196.72	6.5	-35.723	-6.475	-150.76	123.46	25.29
6	700	56.3	-19.46	126.435	6.79	-42.233	-4.351	-101.30	75.75	56.45
7	0	56.3	4.1	279.05	5.81	-25.586	-8.222	-191.43	202.338	10.95
8[1]	715	56.3	-1.69	279.846	6.2	-30.989	-8.796	-204.80	201.463	14.32
9[1]	3	56.3	6.43	300.288	5.63	-23.295	-8.571	-199.56	224.112	9.088
10	315	56.3	-49.75	25.163	-174.19	278.287	0.741	17.253	208.717	-55.252
11	0	56.3	4.1	279.05	5.81	-25.586	-8.222	-191.43	202.338	10.95
12	8	56.3	13.28	300.24	5.0	-16.988	-7.608	-177.14	228.513	5.339
13[2]	5	56.3	8.73	271.923	5.43	-22.348	-7.491	-174.413	197.103	8.585
14	315	56.3	-49.75	25.163	-174.19	278.287	0.741	17.253	208.717	-55.252
15	315	56.3	-49.75	25.163	-174.19	278.287	0.741	17.253	208.717	-55.252
16	158	56.3	148.36	71.147	-20.22	48.94	7.154	166.567	174.871	-29.78
17	180	56.3	166.38	65.273	-19.16	48.207	6.232	145.10	166.387	-23.86
18	200	56.3	183.85	56.573	-16.66	41.236	4.719	109.873	146.436	-16.207

[1] Peak pressure occurs 2° after TDC.
[2] Peak pressure occurs 12° after TDC. All other cases: Peak pressure occurs 7° after TDC.

Note: - Angles β and θ are positive clockwise at C_1 with C_1C_2 as reference. See Fig. 2-7.

- Angle Ψ is positive clockwise at C_2 with C_2C_1 as reference. See Figure 2-7.

TABLE 2.2a

MAXIMUM CYCLIC STRESSES FOR 1 $^{7}/_{8}$-INCH DIAMETER BOLT
CONNECTING ROD IN BOLT 1 REGION

Load Cases	Cyclic Stress (ksi)	Element/ Integration Point	Angle with respect to the x-axis
7 and 17	9.88	219 / 7	-49.362°
7 and 16	9.56	219 / 7	-44.750°
7 and 18	9.59	219 / 7	-52.305°
1 and 17	9.67	219 / 7	-38.764°
1 and 16	9.57	219 / 7	-33.945°
1 and 18	9.21	219 / 7	-42.637°

See Figure 2-9 for location of elements and integration points.

TABLE 2.2b

MAXIMUM CYCLIC STRESSES FOR 1 $^{1}/_{2}$-INCH DIAMETER BOLT CONNECTING ROD NEAR BOLT 1 REGION

Load Cases	Cyclic Stress (ksi)	Element/ Integration Point	Angle with respect to the x-axis
7 and 17	9.012	219 / 7	-57.80°
7 and 16	8.566	216 / 7	-56.49°
7 and 18	8.830	219 / 7	-58.97°

See Figure 2-9 for location of elements and integration points.

TABLE 2.3a

AXIAL STRESSES IN THE BOLTS OF THE 1 $^{1}/_{8}$-INCH DIAMETER BOLT CONNECTING ROD

Load Case Number	Average Axial Stress in ksi		
	Bolt 1	Bolt 2	Lower Bolt
0	32.51	32.51	32.51
7	32.80	32.58	33.03
1	32.90	32.51	33.09
17	32.38	33.14	32.47
16	31.94	32.99	32.13
18	32.29	32.61	32.21
4	32.86	32.58	33.08
12	32.62	32.61	32.91
10	33.99	33.29	32.57
8	32.70	32.58	32.96
13	33.23	32.90	33.44
Maximum Stress Range ($\Delta\sigma$ max)	2.05	0.78	0.96
For Load Cases	10 and 16	10 and 1	1 and 16

TABLE 2.3b

AXIAL STRESSES IN THE BOLTS OF THE 1 $^{1}/_{2}$-INCH DIAMETER BOLT CONNECTING ROD

Load Case Number	Average Axial Stress in ksi		
	Bolt 1	Bolt 2	Lower Bolt
0	50.81	50.81	50.81
7	51.05	50.90	51.33
16	50.26	51.32	50.45
17	50.37	51.15	50.46
18	50.60	50.94	50.52

TABLE 2.4

ENGINE OPERATING HOURS

Percent Load	Peak Firing Pressure	Hours of Crack Growth Lifetime
100%	1579 psig	200 hr
85%	1485 psig	248 hr
75%	1414 psig	286 hr

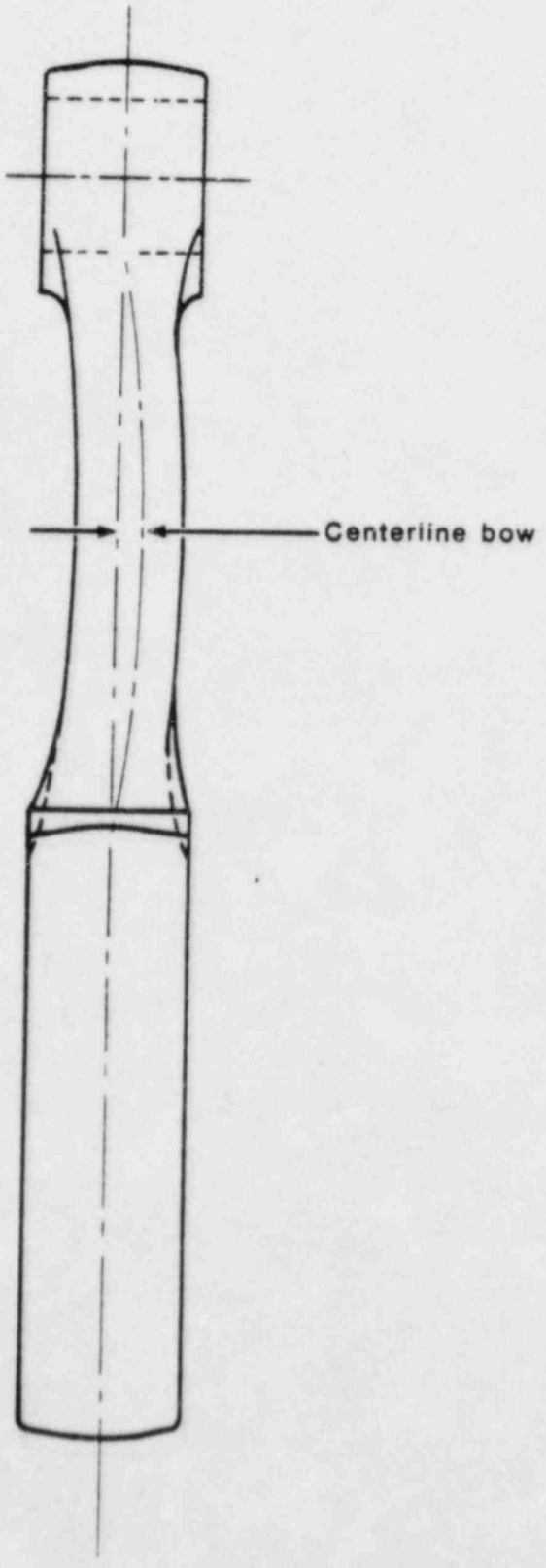

Figure 2-1. Schematic of connecting rod bow.

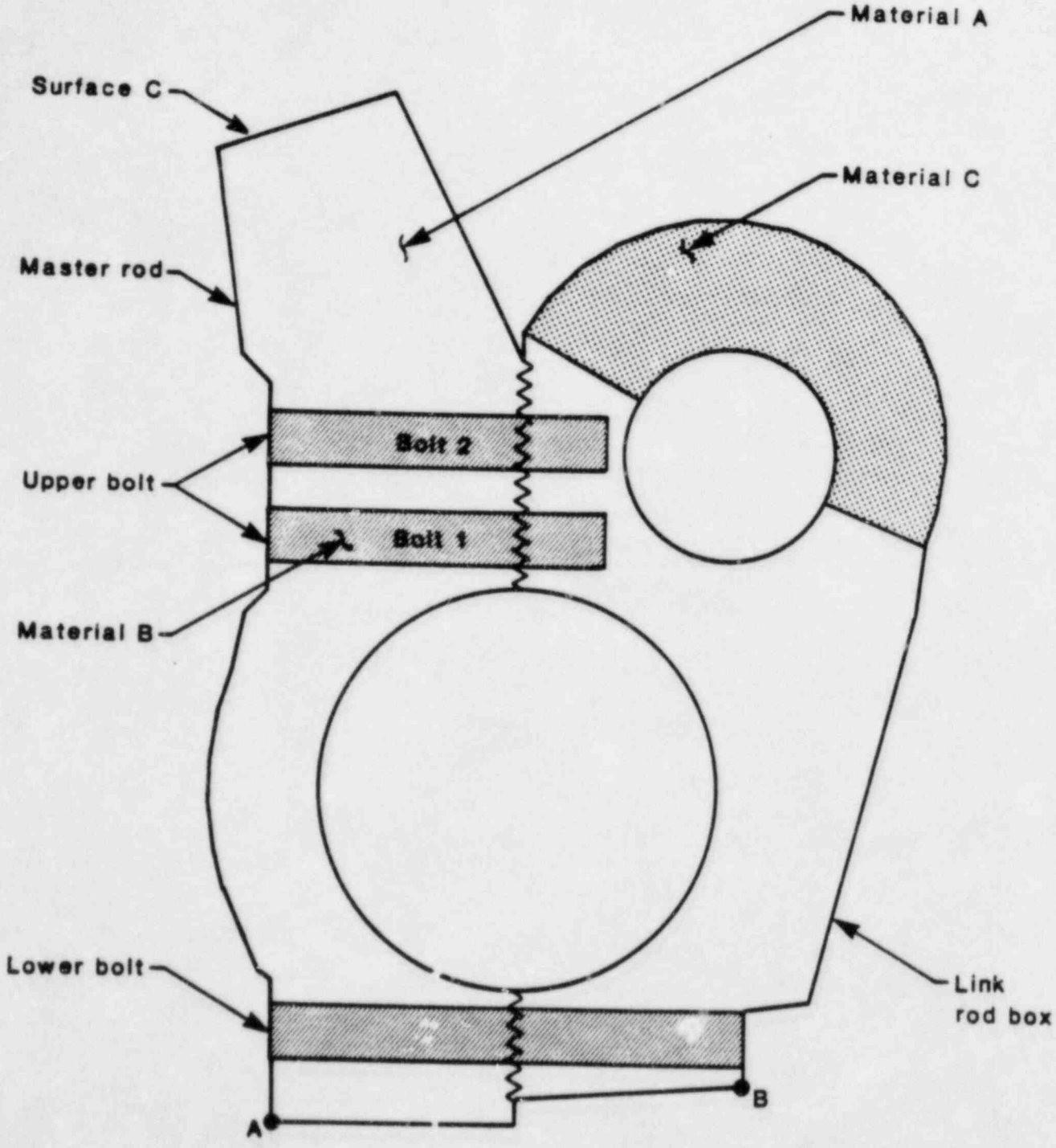

Figure 2-2. V-engine connecting rod assembly.

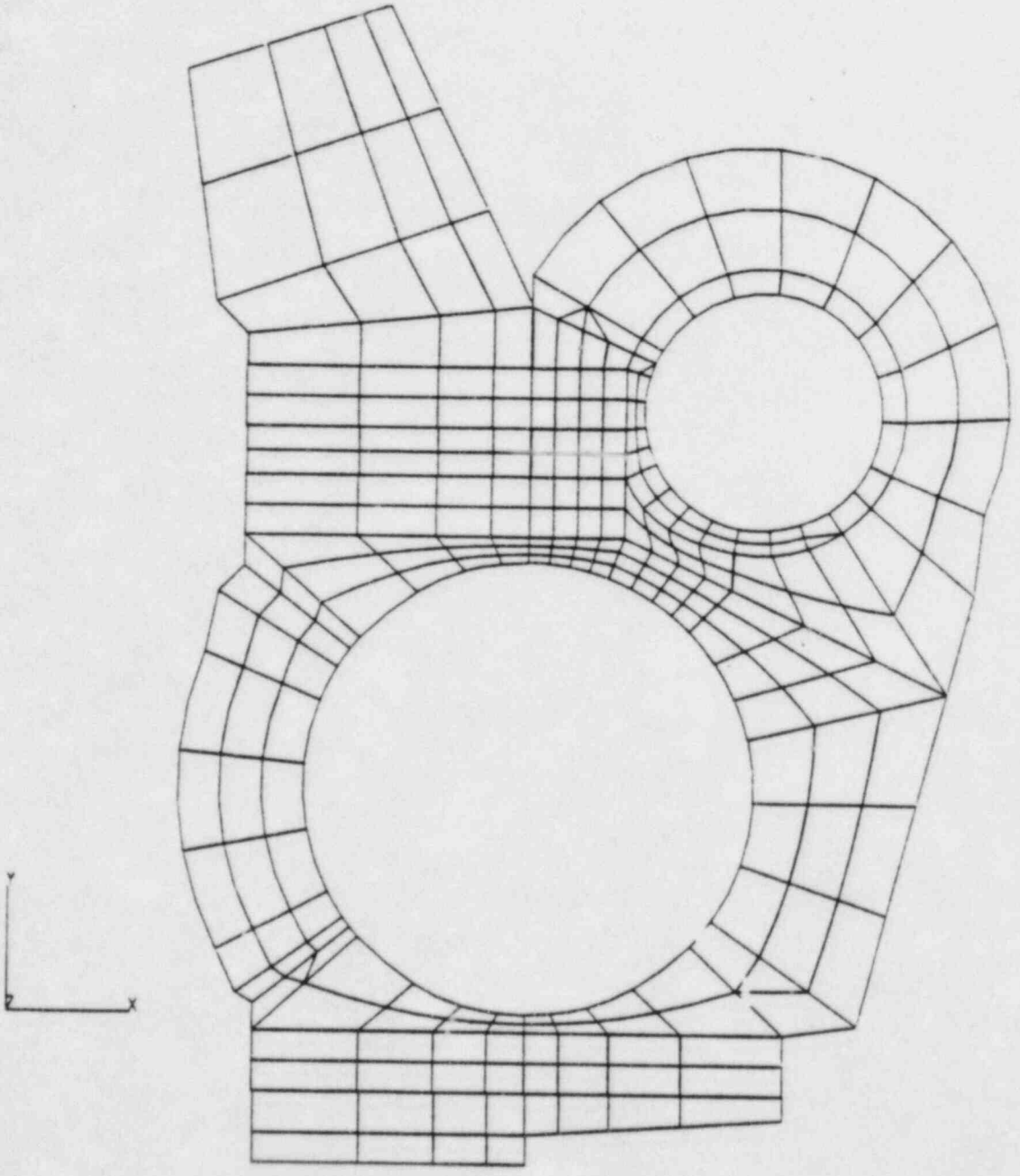

Figure 2-3. Finite-element model of connecting rod.

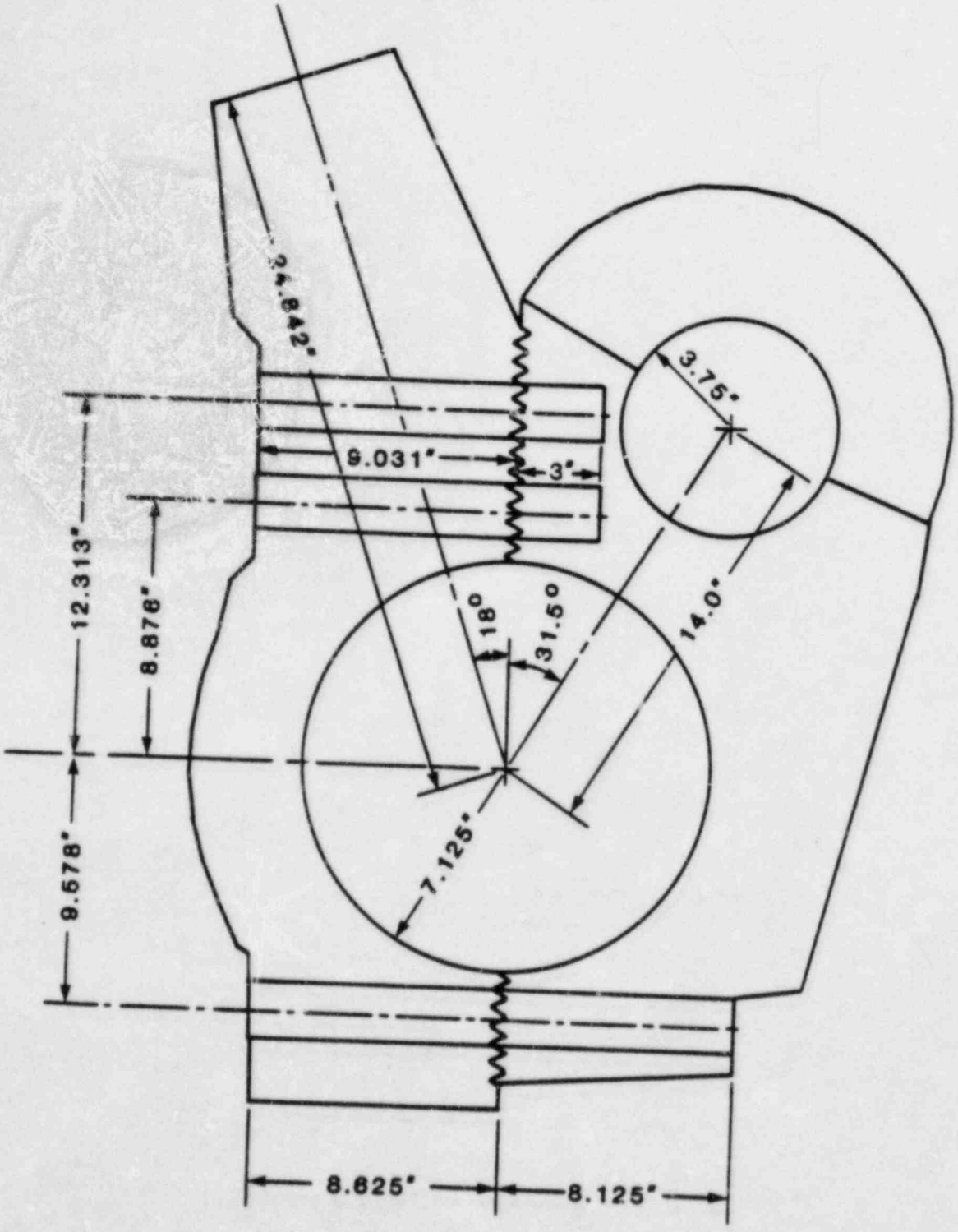

Figure 2-5. Main structural dimensions in inches.

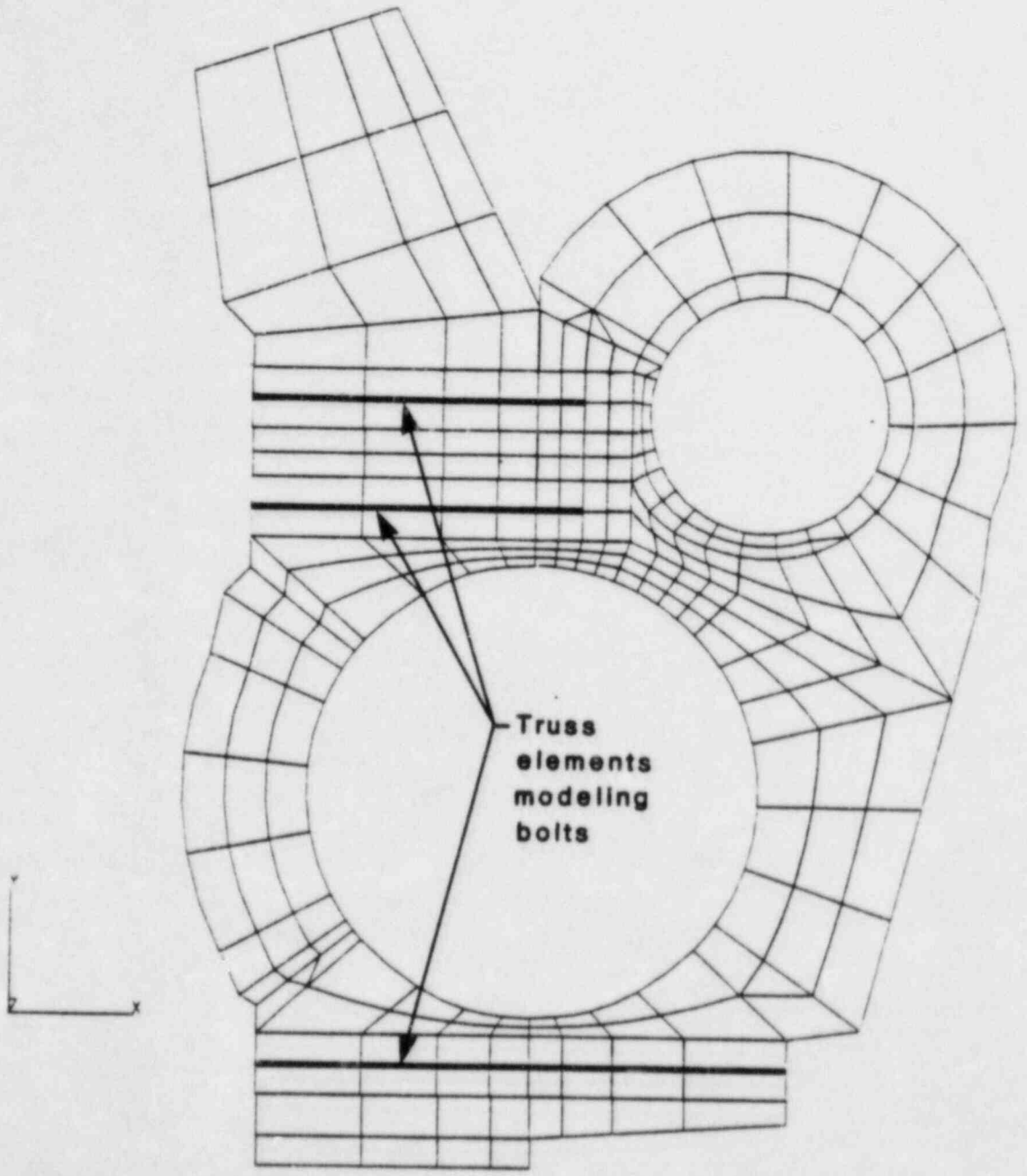

Figure 2-4. Modeling of bolts and bolt-prestress force.

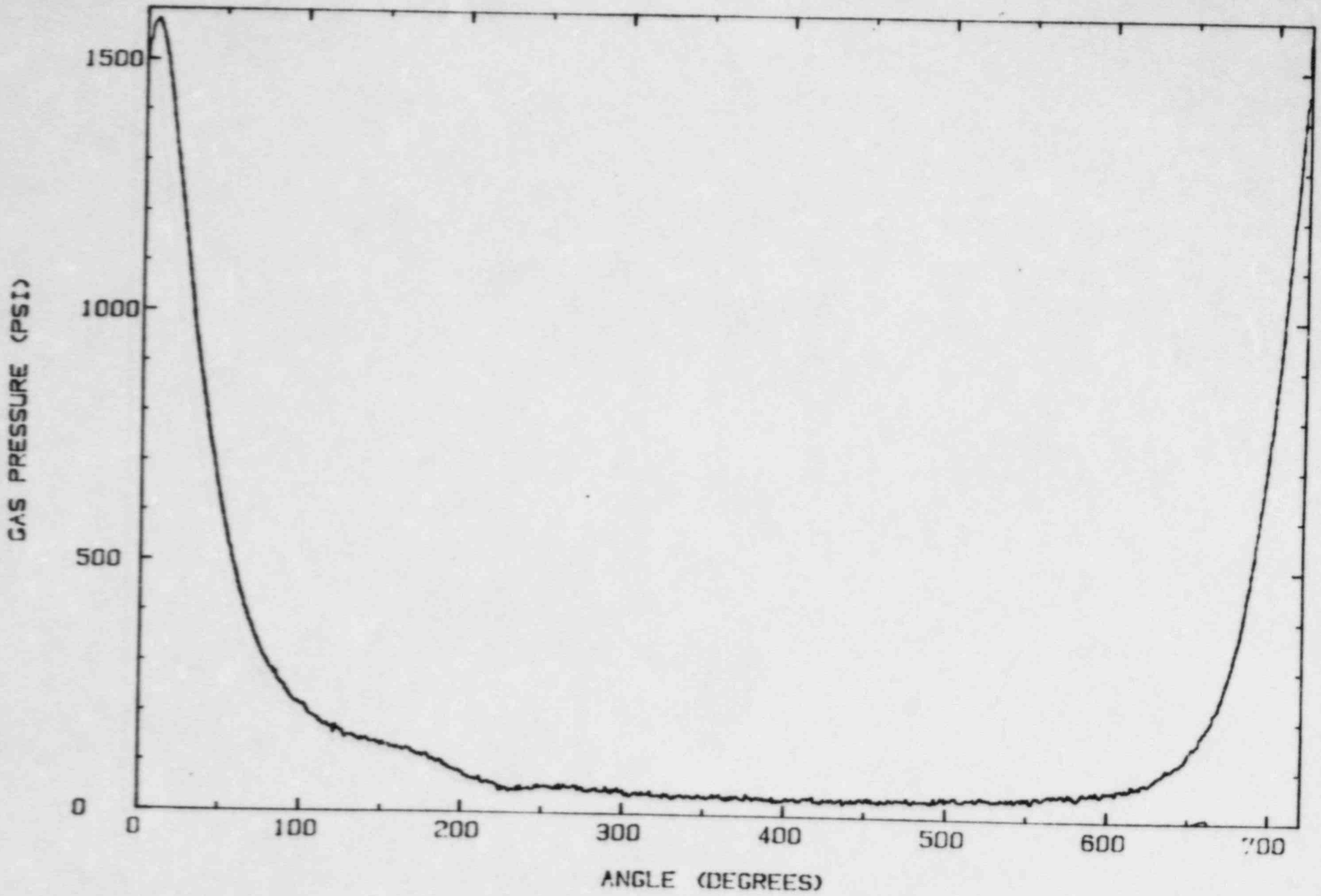

Figure 2-6. Gas pressure versus crank angle (0^{o} corresponds to top dead center).

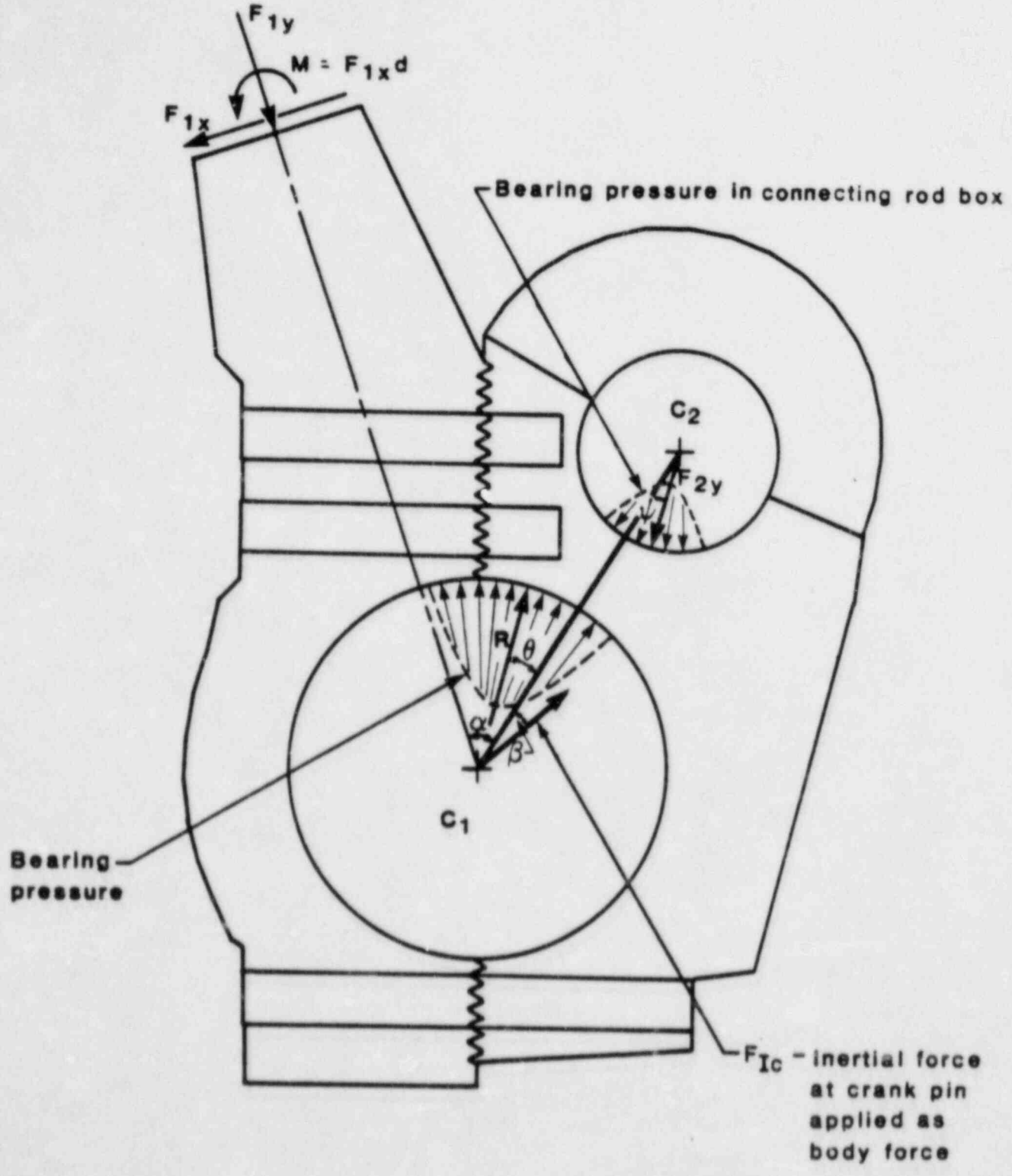

Figure 2-7. Loads acting on the connecting rod.

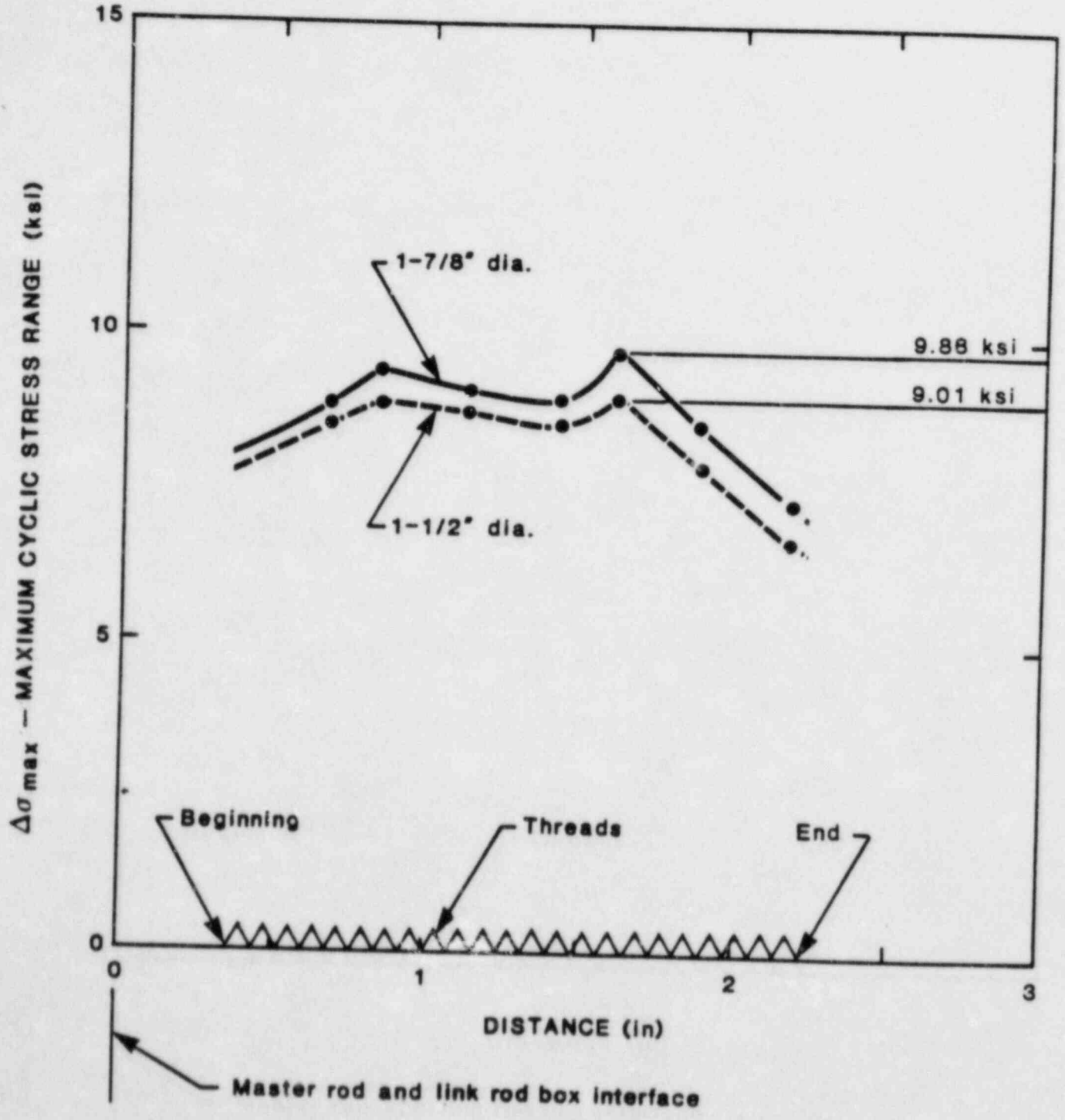

Figure 2-8. Maximum cyclic stress range at bolt hole (Bolt 1).

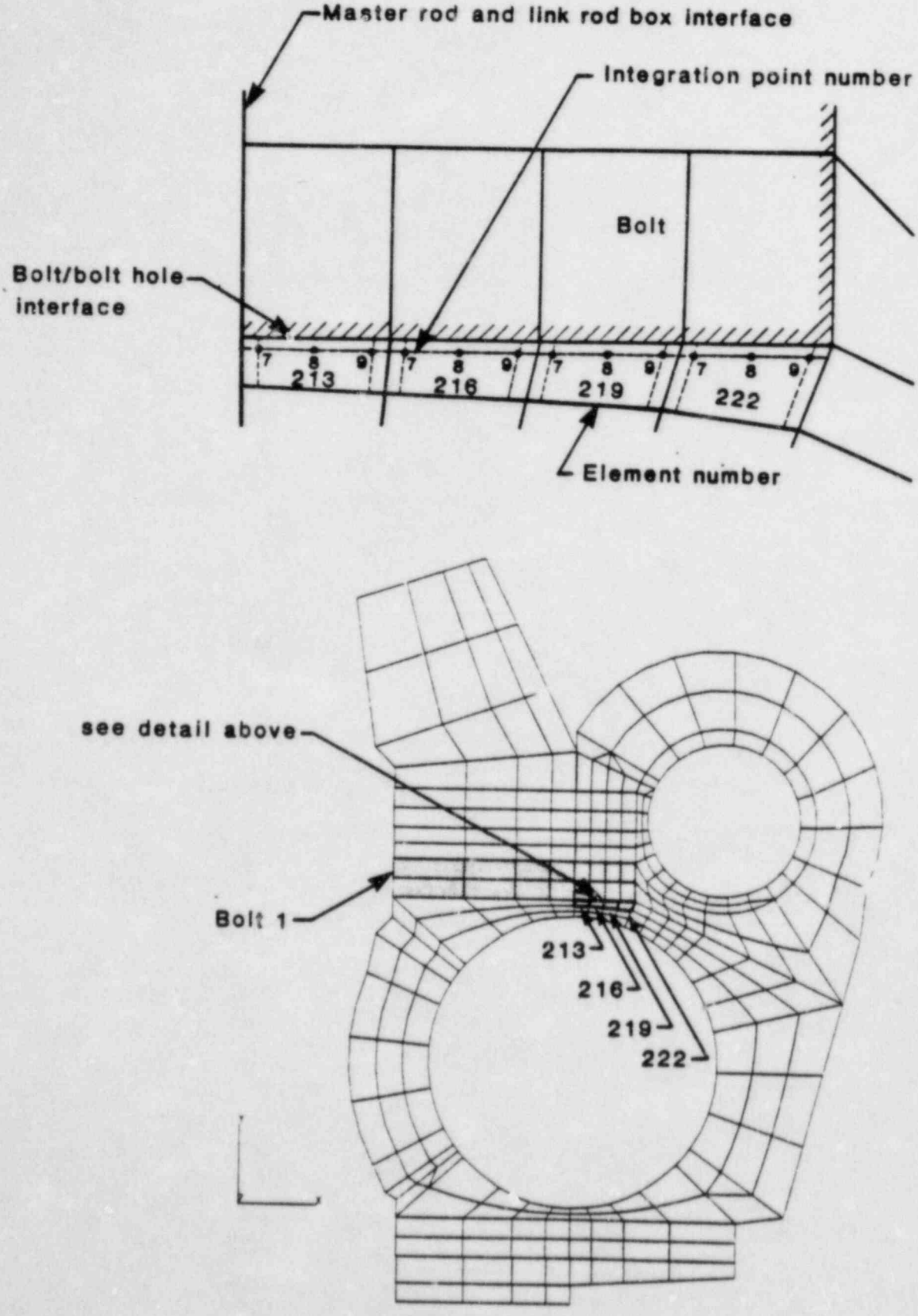

Figure 2-9. Locations of elements of interest in the finite element model of connecting rod.

3.0 CONCLUSIONS

Based on the design review, FaAA concludes that the connecting rods for the TDI DSRV-4 Series engines are adequate for their intended service under the conditions specified below.

3.1 Link Pin Locating Dowel Interference

Clearance between the link pin and link rod should be examined. SIM 349 recommends that this dimension be checked with a 0.0015 inch feeler gage. This dimension must be zero when the specified bolt of 1050 ft-lb is applied.

3.2 Rod Bow

The maximum permissible centerline bow in an H-section connecting rod is 0.47 inch based upon a calculation of axial misalignment under firing pressure. This allowable dimension should be verified.

3.3 Connecting Rod Bolts and Bolt Holes

The first pair of bolts above the crank pin should be removed and inspected by magnetic particle method and the threads of the hole examined for cracking by eddy current or other methods. The allowable time at full load between inspections based upon the reliability of the eddy current inspection is 200 hours. This time assumes that the specified assembly torque is adequate to prevent separation along the serrated joint. Adequacy of the torque depends upon the initial fit between the mating surfaces. It has not been possible to quantify the effect of manufacturing tolerances on this fit. A joint that has been assembled with less than uniform contact may result in loss of bolt preload during operation and consequent fatigue failure. Breakaway torque should be measured and complete dimensional checks of both surfaces made if the breakaway torque is less than 1600 ft-lb for the 1 $^{1}/_{2}$-inch diameter bolts or less than 2400 ft-lb for the 1 $^{7}/_{8}$-inch diameter bolts. As additional experience is accumulated it may be possible to relax the inspection requirements.

3.4 Rod Eye

The rod-eye of the link rod and the rod-eye bushings are similar to those in the inline DSR-48 connecting rods and are subject to the same maintenance procedures recommended for those rods.

APPENDIX A

DERIVATION OF PISTON ACCELERATION FOR V-ENGINE ARTICULATED ROD CONFIGURATION

In this appendix, the dynamic loads that act on the connecting rods are determined by lumping the appropriate masses at the two pistons and the crank pin. Inertial loads are determined by first evaluating the motion of the pistons and the crank pin center. The center of the crank pin has a simple circular motion; therefore, the only inertial load will be that of the radially outward centrifugal force equal to:

$$F_{I_C} = m_c \omega^2 R$$

where

m_c = the mass lump at the crank pin
ω = the angular acceleration
R = the radius of rotation.

The motion of the piston is more complex. However, for a given crank angle, ωt, the position of the pistons can be analytically assessed from the known kinematics. The acceleration of the pistons are determined by differentiating the position of the pistons with respect to time. The pistons undergo a one-dimensional motion along the centerlines of the cylinders.

Consider the schematic description of a V-engine shown in Figure I-1, where the symbols designate:

P_1 = the master rod piston
P_2 = the link rod piston
C_1 = the center of the crank pin
O = the center of the crank shaft
C_2 = the center of the link pin
ℓ_1 = the master rod length
ℓ_2 = the distance between centers of the crank pin and link pin

ℓ_3 = the link rod length

R = the distance between the centers of the crank shaft and crank pin

α = the fixed angle between $P_1C_1C_2$

θ_o = the V-engine angle

ωt = the crank angle

y = the cartesian coordinate along the centerline of the articulated rod cylinder.

x = the coordinate normal to y

C_1', C_2', P_1', P_2' designate the locations of C_1, C_2, P_1, P_2 for a crank angle of ωt.

γ = the angle between OP_1' and $C_1'P_1'$

η = the angle between the y axis and $C_2'P_2'$

Ψ = the angle between $C_1'C_2'$ and $C_2'P_2'$

β = the angle between a radial line OC_1' and C_1C_2'

γ, η, ψ, β are all functions of the crank angle.

Coordinates of C_1'

Coordinates of C_1' are given by:

$$x = R \sin\omega t \tag{A.1}$$

$$y = R \cos\omega t. \tag{A.2}$$

Coordinates of P_1'

Coordinates of P_1' are given by:

$$x = -r_1 \sin\theta_o \tag{A.3}$$

$$y = r_1 \cos\theta_o \tag{A.4}$$

where

r_1 = the distance from the center of the crank pin to the master rod piston, OP_1'.

$$\ell^2_1 = (R \sin\omega t + r_1\sin\theta_o)^2 + (R \cos\omega t - r_1\cos\theta_o)^2 \tag{A.5}$$

Solving for r_1:

$$r_1 = R\cos(\theta_o + \omega t) + [\ell_1^2 - R^2 \sin^2(\theta_o + \omega t)]^{1/2} \qquad (A.6)$$

The acceleration of the master rod piston is equal to the second derivative of r_1, which is determined by differentiating Eq. A.5 twice.

Differentiating Eq. A.5 once gives:

$$\frac{dr_1}{dt}\left(r_1 - R\cos(\theta_o + \omega t)\right) + R\omega\, r_1 \sin(\theta_o + \omega t) = 0, \qquad (A.7)$$

from which the velocity $\frac{dr_1}{dt}$ is determined.

$$\frac{dr_1}{dt} = \frac{-R\omega\, r_1 \sin(\theta_o + \omega t)}{\left(r_1 - R\cos(\theta_o + \omega t)\right)} \qquad (A.8)$$

Differentiating Eq. A.7 again gives:

$$\frac{d^2r_1}{dt^2} = \frac{-\left(\frac{dr_1}{dt}\right)^2 + 2R\omega\frac{dr_1}{dt}\sin(\theta_o + \omega t) + R\omega^2 r_1 \cos(\theta_o + \omega t)}{r_1 - R\cos(\theta_o + wt)} \qquad (A.9)$$

where $\frac{d^2r_1}{dt^2}$ represents the acceleration of the master rod piston.

Angle γ between $OP_1'C_1'$ for any crack angle is determined from the following two equations:

$$R\cos(\theta_o + \omega t) + \ell_1 \cos\gamma = r_1 \qquad (A.10)$$

$$\ell_1 \sin\gamma = R\sin(\theta_o + \omega t) \qquad (A.11)$$

Hence,

$$\tan \gamma = \frac{R \sin(\theta_o + \omega t)}{r_1 - R \cos(\theta_o + \omega t)} \tag{A.12}$$

To simplify the determination of the motion of the link rod piston, define transformed coordinates x', y' at C_1' origin such that x' is parallel to x, and y' is parallel to y. Then,

$$x = x' + R \sin\omega t \tag{A.13}$$

$$y = y' + R \cos\omega t \tag{A.14}$$

Next, define transformed coordinates x", y" at C_1' origin such that y" is along $C_1'P_1'$ and x" is orthogonal to $C_1'P_1'$.

The rotation angle ϕ between the x' and x" axes is related by:

$$\cos \phi = \frac{r_1 \cos\theta_o - R \cos\omega t}{\ell_1} \tag{A.15}$$

$$\sin \phi = \frac{r_1 \sin\theta_o + R \sin\omega t}{\ell_1} \tag{A.16}$$

Coordinates x" and y" are related to x' and y' by:

$$x' = x" \cos\phi - y" \sin\phi \tag{A.17}$$

$$y' = x" \sin\phi + y" \cos\phi \tag{A.18}$$

Coordinates of C_2'

Coordinates of point C_2' in the x", y" plane are given by:

$$x"_{C_2'} = \ell_2 \sin\alpha \tag{A.19}$$

$$y"_{C_2'} = \ell_2 \cos\alpha \tag{A.20}$$

In the x, y cartesian plane, the coordinates of C_2' are given by:

$$x_{C_2'} = \ell_2 \sin\alpha \cos\phi - \ell_2 \cos\alpha \sin\phi + R \sin\omega t \qquad (A.21)$$

$$y_{C_2'} = \ell_2 \sin\alpha \sin\phi + \ell_2 \cos\alpha \cos\phi + R \cos\omega t \qquad (A.22)$$

Coordinates of P_2'

Coordinates of P_2' can be evaluated from the foregoing two equations:

$$x_{P_2'} = 0, \text{ and} \qquad (A.23)$$

$$(y_{P_2'} - y_{C_2'})^2 + x_{C_2'}^2 = \ell_3^2 \text{ or} \qquad (A.24)$$

$$y_{P_2'} = y_{C_2'} + (\ell_3^2 - x_{C_2'}^2)^{1/2} \qquad (A.25)$$

For brevity, let $y_P = y_{P_2'}$, $x_P = x_{P_2'}$; $x_C = x_{C_2'}$, $y_C = y_{C_2'}$.

A.22 can be written as:

$$(y_P - y_C)^2 + x_C^2 = \ell_3^2 \qquad (A.26)$$

Differentiate above equation with respect to time using dots to designate time differentiation;

$$(y_P - y_C)(\dot{y}_P - \dot{y}_C) + x_C \dot{x}_C = 0 \qquad (A.27)$$

Rearranging Eq. A.27 gives the velocity of the link rod piston:

$$\dot{y}_P = \frac{1}{y_p - y_c} \left[(y_P - y_C)\, \dot{y}_C - x_C \dot{x}_C \right] \tag{A.28}$$

Differentiating Eq. A.27 again produces the link rod piston acceleration:

$$\ddot{y}_P = \ddot{y}_C - \frac{1}{(y_P - y_C)} \left[(\dot{y}_P - \dot{y}_C)^2 + (\dot{x}_C)^2 + x_C \ddot{x}_C \right] \tag{A.29}$$

Time derivatives of $x_{C_2'}$ and $y_{C_2'}$ are determined from Eqs. A.18 and A.19 as follows:

let

$$\cos'\phi = \frac{d}{dt} (\cos\phi) \tag{A.30}$$

Then;

$$\dot{x}_{C_2'} = R\omega \cos\omega t + \ell_2 (\sin\alpha \cos'\phi - \cos\alpha \sin'\phi) \tag{A.31}$$

$$\dot{y}_{C_2'} = -R\omega \sin\omega t + \ell_2 (\sin\alpha \sin'\phi + \cos\alpha \cos'\phi) \tag{A.32}$$

$$\ddot{x}_{C_2'} = -R\omega^2 \sin\omega t + \ell_2 (\sin\alpha \cos''\phi - \cos\alpha \sin''\phi) \tag{A.33}$$

$$\ddot{y}_{C_2'} = -R\omega^2 \cos\omega t + \ell_2 (\sin\alpha \sin''\phi + \cos''\phi \cos\alpha) \tag{A.34}$$

Time derivatives of $\sin\phi$ and $\cos\phi$ are determined from Eqs. A.12 and A.13 by direct differentiation of those equations:

$$\sin'\phi = \frac{1}{\ell_1}\left(\dot{r}_1 \sin\theta_o + R\omega\cos\omega t\right) \tag{A.35}$$

$$\sin''\phi = \frac{1}{\ell_1}\left(\ddot{r}_1 \sin\theta_o - R\omega^2 \sin\omega t\right) \tag{A.36}$$

$$\cos'\phi = \frac{1}{\ell_1}\left(\dot{r}_1\cos\theta_o + R\omega \sin\omega t\right) \tag{A.37}$$

$$\cos''\phi = \frac{1}{\ell_1}\left(\ddot{r}_1 \cos\theta_o + R\omega^2 \cos\omega t\right) \tag{A.38}$$

The angle η between the link rod and the y axis is given by:

$$\tan\eta = \frac{x_{C_2'}}{\left(y_{P_2'} - y_{C_2'}\right)} = \frac{x_{C_2'}}{\left(\ell_3^2 - x_{C_2'}^2\right)^{1/2}} \tag{A.39}$$

Direction of centrifugal force is given by:

$$\beta = \theta_o + \omega t + \gamma - \alpha.$$

Direction of forceacting on the link rod is given by:

$$\psi = \eta + \alpha - \theta_o - \gamma.$$

The combined forces acting on the connecting rod are shown in Figure I-2. On the master rod an axial and horizontal force are exerted. On the link rod, only an axial force is applied. From a simple free body diagram consideration, F_{2_y} is given by:

$$F_{2_y} = \frac{\left(F_{I_2} + F_{g_2}\right)}{\cos\eta}$$

where

F_{I_2} = the inertial force of the mass lumped at the link rod piston.
F_{g_2} = the gas pressure force.

The inertial force equals:

$$F_{I_2} = -m_2 \frac{d^2 y_{P_2}}{dt^2}$$

The acceleration was given by Eq. A.29.

The gas pressure force is determined from the pressure, which is a function of the crank angle times the piston area. This force will be compressive.

The horizontal force acting on the master rod is determined by requiring moment equilibrium at the crank pin center.

$$F_{1_x} = -\frac{\ell_2}{\ell_1} F_{2_y} \sin \psi.$$

The axial force along the master rod is given by equating the sum of the forces along the master rod piston to the gas pressure plus inertial load. That is;

$$F_{I_1} + F_{g_1} = F_{1_y} \cos\gamma - F_{1_x} \sin\gamma$$

or

$$F_{1_y} = \frac{F_{I_1} + F_{g_1}}{\cos\gamma} + F_{1_x} \tan\gamma$$

The reactions at the crank pin (point C_1) are given by force equilibrium:

$$R_x = F_{2_y} \cos\psi + F_{1_y} \cos\alpha - F_{I_c} \cos\beta - F_{1_x} \sin\alpha$$

$$R_y = F_{2_y} \sin\psi + F_{1_y} \sin\alpha + F_{I_c} \sin\beta + F_{1_x} \cos\alpha$$

where

F_{I_c} = the inertial force due to the lumped mass at the crank pin center.

R_x and R_y are the components of the reaction at the crank pin hole.

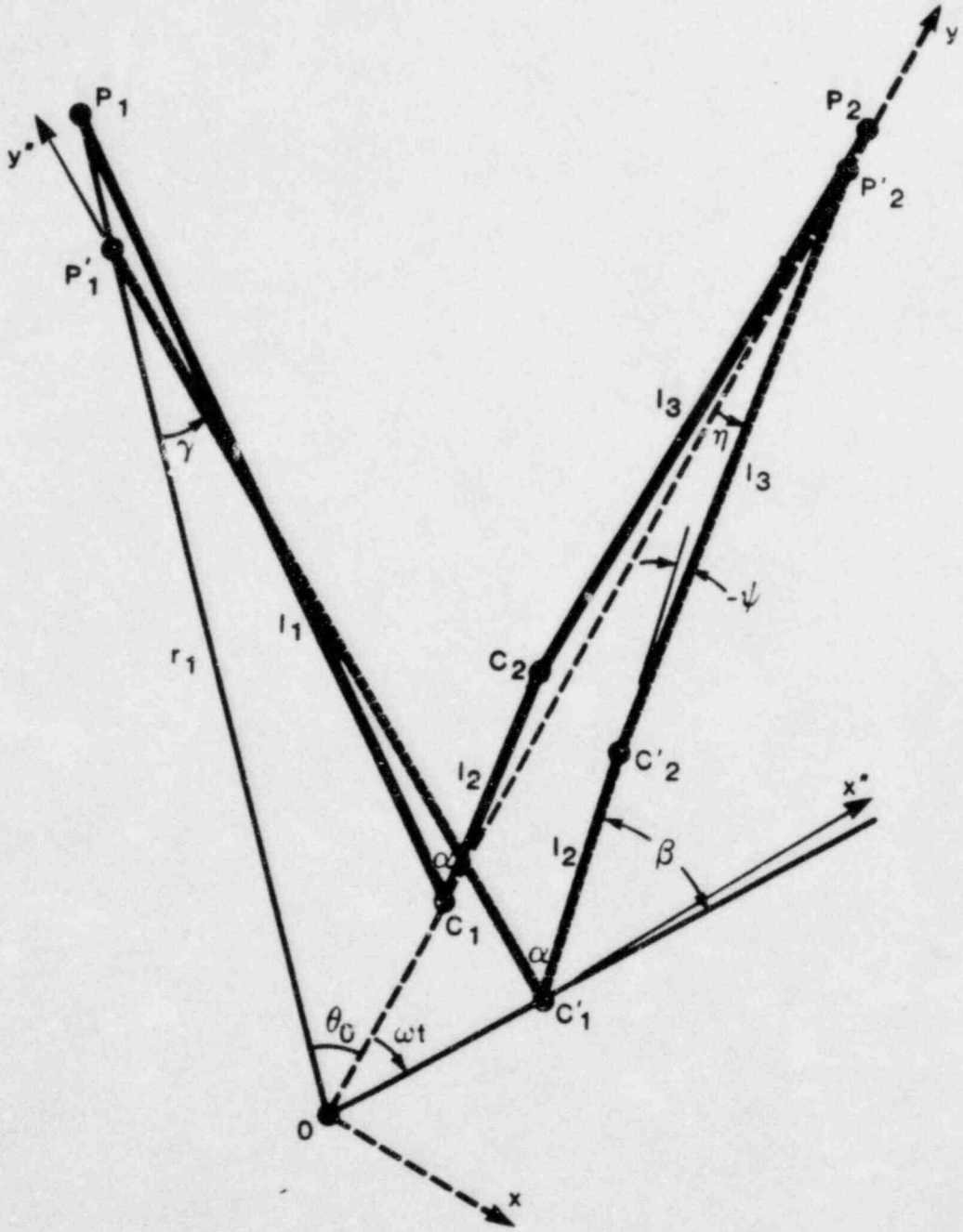

Figure A-1. Kinematics of V-engine connecting rods.

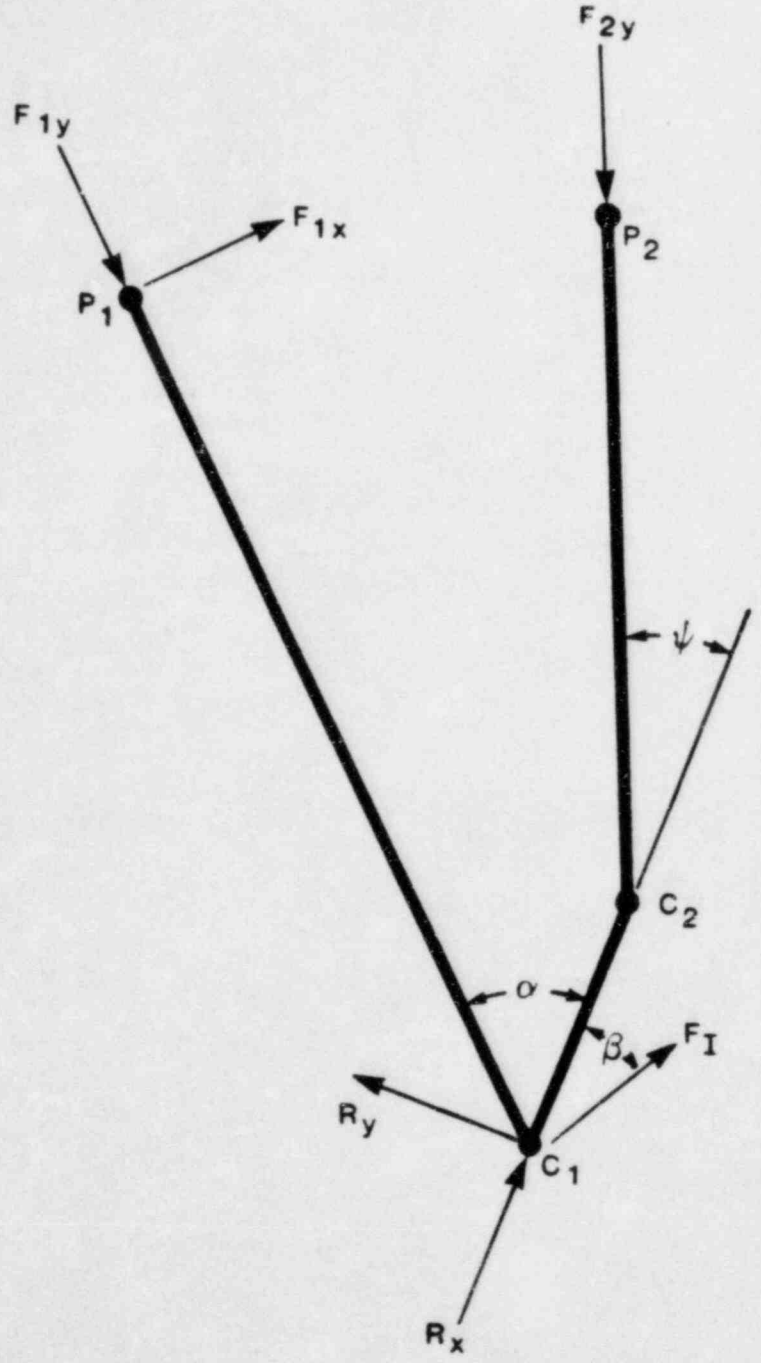

Figure A-2. Free body diagram of actions and reactions on the V-engine connecting rod.

APPENDIX B

COMPONENT DESIGN REVIEW
TASK DESCRIPTION

CONNECTING ROD
PART NO. 03-340A

Classification A
Completion 3/20/84

PRIMARY FUNCTION: The connecting rod transmits engine firing forces from the pistons and piston pins through the rods to the crankshaft such that the reciprocating motion of the pistons induces rotation and output torque of the crankshaft.

FUNCTIONAL ATTRIBUTES:

1. The connecting rod must have sufficient column buckling strength and fatigue resistance to withstand cylinder firing forces and inertial loads.
2. In the RV engine design, the three oscillating bearings two (2) wrist pin bearings and one (1) link pin bearing and the rotating crank pin bearing all require support from the connecting rod. In the R-48 design, a single wrist and crank pin bearing are supported. The flexure of the rod must be such that bearings are not unacceptably distorted.
3. Passages within the rod must provide cooling and lubricating oil to the bearings and pistons.
4. Stress levels, both mean and alternating, must fall within the endurance limits for the material utilized.
5. In the RV design, the two bolted joints (link rod to link pin and master rod to link rod box) must maintain sufficient contact pressure. The R-48 design likewise requires sufficient clamping forces on the crank pin bearing cap.
6. The rod cap bolts must support the necessary preload without yielding, fracture or unacceptable thread distortion.

7. The wrist pin (or rod-eye) bushing must acceptably support the gas pressure and inertia forces transmitted by the pistons during the unique nuclear standby required starting cycle and normal operation.

SPECIFIED STANDARDS: None

EVALUATION:

1. Determine the service histories of the connecting rods. In particular, evaluate the two V-style connecting rods (the 1 $^{7}/_{8}$-inch bolt diameter connecting rod and the 1 $^{1}/_{2}$-inch bolt diameter rod) and the R-48 style connecting rod.
2. Incorporate firing load profile data for the crankshaft analysis and the results of the 13-inch diameter rod bearing analyses to produce a connecting rod static load profile, with the addition of inertia loads for a complete time-load map.
3. Evaluate the significance of possible rod bow as it affects bearing centerline angular misalignment.
4. Review and report on failure of connecting rod at Copper Valley Electric, Glenn Allen, Alaska.
5. Conduct journal orbit analysis of the wrist pin bearing.
6. Using examples of fractured rods to focus the area of investigation, develop finite element models of the 1 $^{7}/_{8}$-inch bolt diameter V-type rod, to define deformation and the possibility of crack initiation and propagation.
7. Evaluate the necessary preload and acceptable design requirements (yielding, thread distortion) of the rod cap bolts for the R-48 and RV designs.
8. Evaluate the loading, fabrication and installation requirements of the wrist pin (or rod-eye) bushing for acceptable nuclear standby service.
9. Perform a metallurgical examination of fractured connecting rods in FaAA possession.
10. Complete final report.

REVIEW TDI ANALYSIS:

1. Review any TDI stress analyses or strain gage testing of connecting rods.

INFORMATION REQUIRED:

1. Connecting rod, wrist pin bearing and cap bolt drawings.
2. Engine operating parameters (i.e., speed, firing pressure time history, etc.).
3. Component physical parameters (piston weight, connecting rod reciprocating and rotating weights, etc.).
4. TDI specified rod cap bolt torques and installation procedures.
5. TDI failure history of DSR-48 and DSRV connecting rods.
6. Bushing and connecting rod material specifications.